Effect of Janus Particles on Performance of Electroactive Polymer Films

By

Hsinyu Chen

A Dissertation submitted to the Graduate Faculty in Engineering in Partial Fulfillment of the Requirements for the Degree of Doctor of Philosophy, The City University of New York

2013

This manuscript has been read and accepted for the Graduate Faculty in Engineering in satisfaction of the dissertation requirement for the degree of Doctor of Philosophy.

September 4th, 2013

Date

Chair of Examining Committee
Prof. Ilona Kretzschmar, Associate Professor,
Department of Chemical Engineering,
The City College of New York

September 4th, 2013

Date

Executive Officer
Prof. Ardie Walser

Prof. Alexander Couzis — Professor, Department of Chemical Engineering
The City College of New York

Prof. Raymond Tu — Assistant Professor, Department of Chemical Engineering
The City College of New York

Prof. Niell Elvin — Associate Professor, Department of Mechanical Engineering
The City College of New York

Prof. Alan Lyons — Professor, Department of Chemistry
College of Staten Island

Supervisory Committee

THE CITY UNIVERSITY OF NEW YORK

Abstract

Effect of Janus Particles on Performance of Electroactive Polymer Films

By

Hsinyu Chen

Advisor: Ilona Kretzschmar

Dielectric elastomers (DEs) have become a popular material, because they can efficiently convert between electrical and mechanical energy. This property enables their use as electromechanical actuators in applications such as mini-robots, artificial muscles, or dynamic tactile screens. Owing to the reversibility of the mechanical-to-electrical energy conversion, DEs can also be employed in modern green energy technology to harvest natural forces from wind and ocean waves to generate green energy thereby satisfying a continuously increasing energy demand.

The dielectric elastomer, poly(ethylene glycol phenyl ether acrylate), p(EGPEA) for short, is used in this thesis. p(EGPEA) responds according to the Maxwell effect when stressed, i.e., the strain is proportional to the dielectric constant and the square of the external electric field and inversely proportional to its Young's Modulus. p(EGPEA) is a soft polymer with a dielectric constant (6.59 at 20 Hz) that shows an actuation in the 0~2 % range at external fields of 12 V/m. This low actuation response at these relatively high actuation fields limits its applicability in technology that involves interfaces with humans. One way to improve the electromechanical actuation is the increase of p(EGPEA)'s dielectric constant and/or lowering of its Young's

Modulus through the addition of fillers, i.e., materials with higher dielectric constants or lower Young's Moduli, respectively.

One kind of filler particle is the Janus particle, a particle that carries a metallic cap on one half of its surface. Janus particles are interesting filler particles due to their anisotropic structure. Here, 500 nm SiO_2 particles are assembled into monolayers and coated with 5/20 nm Ti/Au on one hemisphere. 0.5 vol% of the resulting Janus particles are added to the p(EGPEA) films and their effect on the Young's Modulus, the dielectric constant, and the actuation behavior of p(EGPEA) is studied. Interestingly, an astonishingly high overall dielectric constant of 10.20 for JP SiO_2-loaded p(EGPEA) composite films at 20 Hz compared to the ε_r-value of 6.59 for pure p(EGPEA) is measured. Most surprisingly, addition of 0.5 vol% Janus particles results in an unexpected lowering of the Young's Modulus, an observation that does not agree with the mixing theory of Guth and Simha.

An additional set of experiments ranging from swelling via UV/Vis spectroscopy and thermogravimetric analaysis (TGA) to nanoindentation measurements is used to better understand the effect of the gold caps on the curing behavior and the dielectric constant. We find that the presence of gold caps contributes to the inhibition of the 365 nm UV light exposure resulting in a less thoroughly crosslinked and softer polymer in the vicinity of the caps. Further, we also show that the enhancement of the dielectric constant cannot be explained by the reduced curing alone, but that it also has to involve the anisotropic nature of the Janus particles.

Owing to the larger dielectric constant and the decreased Young's Modulus, the electrostriction coefficient of JP SiO_2-loaded p(EGPEA) composite films is measured as S_{exp} = 55×10^{-16} m^2/V^2 compared to that of pure p(EGPEA) films $S_{exp} = 0.69\times10^{-16}$ m^2/V^2 indicating a 10

times stronger response or a potential reduction in the actuation E-field required to obtain the same electromechanical strain response. Discrepancy is found between the measured S_{exp} and theoretical S_{theo} values calculated from the Y and ε_r values pointing towards a potentially more complex electrostriction mechanism.

Acknowledgements

First of all, I would like to express my gratitude to my doctoral mentor, Prof. Ilona Kretzschmar, not only for her professional guidance but also for her moral and emotional support. She gave me a lot of support in the very beginning of my graduate life in the US. Her passion and dedication to my work has given me the needed encouragement to overcome many challenges and setbacks during my doctoral research. Most importantly, I really appreciate that she taught me how to be an independent, brave, and confident person in all respects during my life in United States.

In addition, I would like to thank all my PhD committee members, Prof. Raymond Tu, Prof. Alexander Couzis, Prof. Niell Elvin, and Prof. Alan Lyons for their professional advice and kind guidance to improve my work throughout this thesis.

A special thanks goes to Dr. Ashok Maliakal and Dr. Jingqin Cui not only for their experimental help but also for their inspiration and for introducing me to the exciting topic of actuation at the beginning of this project.

Further, I would like to thank Dr. Shuangyi Liu (capacitance measurement), Prof. Sihong Wang (Optical surface profiler), Prof. Youngsik Song (DEKTAK profiler), Prof. Gabriel Tardos (texture analyzer), Prof. Alan Lyons (capacitance measurement), Prof. Alexander Couzis (nanoindentation and FTIR), Dr. Junshe Zhang (TGA), Mr. Kunal Savaji (nanoindentation), Mr. Julian Silverman (UV/vis) for their experimental guidance and availability for scientific discussions. Also, I would like to thank Mr. Andy Eng, Mr. Zhengrong Xu, Ms. Lisa Taylor, and Ms. Mary Wright for their administrative and technical support.

Further, I would like to acknowledge NSF award #0651747 and the City College of New York FY 12 City Seed Award for funding of my research stipend and the materials and supplies needed to carry out this thesis work. Further, CUNY's Doctoral Student Research Grants competition #5 is acknowledged for support of my travel to the 2011 AICHE conference allowing me to present parts of this Thesis to a scientific audience.

In the end, I would like to thank my lab colleagues: Kevin, Amar, Roger, Sepideh, Alex, Julius, Naomi, Dane, Evgeyniya, and Mamadou for their kind help and passionate discussions on every single day in the lab. Especially, I would like to thank my close friends and roommates, Xia, Xue, Xiaoxiao, Bin, Sonia, Zhenping, Weikang, Iwen, Katy, Tzu-Chia, Peggy, Chia-en, Yiguo, Luhan, Yvonne, Sinru, Emily, Shiyu, Chiew, Leo, Chris, Shu, and Esther for their company over the years and their ability to listen when I needed them. They have enriched my life and have filled it with love and joy.

Most importantly, I would like to thank my parents and the extended Chen family; Charlene, Yao-Kun, Tammy, George, Tina, Sandy, Philip, Eric, Chris, Joanne, and Grandmom for their respect and undying support to finish my doctoral studies and their continuous encouragement to chase my dreams. I would have never completed my PhD studies without their support and love.

Hsinyu Chen

August 2013

Table of Contents

List of Tables

List of Figures

Chapter One – Introduction

Society's energy demand has been increasing continuously and rapidly. To satisfy the human need for energy, alternative green energy sources, such as wind or ocean waves, have become interesting alternatives to contribute to the overall energy supply. Therefore, the question of how to efficiently convert such wind/ocean forces into electric energy has become an important one. In this thesis, we explore a new material, i.e., a dielectric elastomer with Janus particle fillers, which could potentially enable the efficient conversion of mechanical energy (wind/ocean force) to electric energy. In addition, the reverse energy conversion from electrical to mechanical energy is also possible and could be employed in applications such as artificial muscles, mini-robots, or tactile displays.

1-1 Electroactive Polymers (EAPs)

Electroactive polymers (EAPs) are materials that respond to external electric stimulation by changing their shape or size. This expanding and contracting characteristic of EAPs can be applied in, for example, an artificial muscle where the applied voltage controls the shape change. More generally, advantageous properties of EAPs are their light weight, portability, and low cost due to the properties of the polymers. Also, EAPs are potential materials for actuators and sensors because they can convert electric energy into mechanical deformation rapidly.

Electroactive polymers (EAPs) are classified into two types, i.e. ionic and electronic, based on their actuation mechanism. There are four main types of ionic EAPs; (i) carbon nanotubes (CNTs), (ii) conjugated polymers (CPs), (iii) ionic polymer-metal composites (IPMCs), and (iv) ionic polymer gels. The actuation of ionic EAPs is caused by the diffusion of

charge carriers, which requires an electrolyte. Because they need an electrolyte, most ionic EAPs are hydrated and wet during operation. The advantage of ionic EAPs is that they require a low driving voltage (~1V) and exhibit a high current density. Their disadvantage is caused by their diffusion-based mechanism resulting in a low actuation speed and a low efficiency (~1%).[1]

In contrast to ionic EAPs, electronic EAPs are operated under dry conditions.[2] Electronic EAPs do not need an electrolyte due to the fact that their actuation mechanism is based on electrostatic attraction. The main advantage of electronic EAPs is their low power consumption allowing them to be used for a longer time compared to ionic EAPs.[2] Their response time is less than 10^{-3} s under DC voltage, which is very fast.[2] The measured strains are around 40 to 60 %.[2] The energy density in electronic EAPs can be as high as 50 J/cm^3. They do not need an electrolyte as there is no charge diffusion. However, they require an activation field as high as 150 V/m,[1] which is close to the breakdown level of most polymers. In addition, the actuation force is often too low to afford a heavy load, ranging from 0.1~ 25 MPa.[3]

When ionic and electronic EAPs are stimulated, two types of actuation strains are usually generated; the tensile/compressive strain and bending strain as depicted in Figure 1-1. The bending strain shown in Figure 1-1 (b) is caused by the structure of the polymer and the arrangement of the molecules. It originates from a decrease or increase of the molecular density on one side of the sample or by a decrease or increase of the inter- or intra-molecular distance. For example, the strains experienced by ionic EAPs belong to this type. Deformation due to tensile strain as shown in Figure 1-1 (c) is caused by application of a uniform compressive stress in the plane of the polymer film, which is perpendicular to the applied voltage.

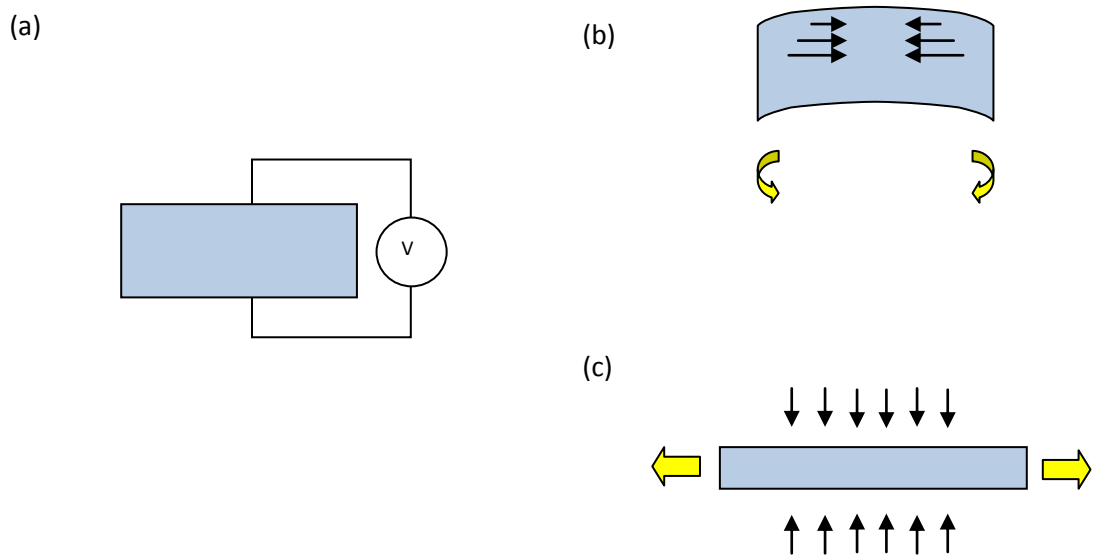

Fig. 1-1 Strains observed during EAP actuation: (a) EAP before application of external DC voltage, (b) EAP exhibiting a field-induced bending strain, and (c) EAP showing field-induced tensile/compressive strain.

1-2 Filled Electronic EAPs

Currently, the major factor hampering the application of electronic EAPs is that electronic electroactive polymers require very high fields to obtain the required expansion for tactile detection or large external force to obtain the required compression for energy harvesting. The two key criteria for application of electronic EAPs are the ability to maintain the flexibility and speed of response of soft polymers, while also increasing the dielectric coefficient to increase the achievable strain to a detectable limit. A composite material usually carries properties of all components with strong enhancement of certain properties at low filler concentrations.[4] In the case of electronic EAPs, the composite of a soft polymer with low Young's Modulus and high dielectric coefficient filler particles could lead to increased strain values in decreased actuation fields.

1-3 Applications: Power Generators and Braille Displays

Based on the mechanism of electronic EAPs, electro-mechanical actuators can convert between electrical and mechanical energy. In other words, there are two main types of applications; one is energy harvesting in which the power is generated by the deformation of the generators due to an external force, while the other is a Braille display in which the actuators deform to compress or bend due to the addition of an external electric energy. We will introduce more details of these two major applications in the following.

1-3-1 Power Generators[5]

Electroactive polymer based power generators are environment friendly energy harvesting devices such as tidal or wave power plants, which are located near the seashore using the kinetic energy of the ocean currents for energy generation. The design of this type of power generators consists of several elastomeric rolls connecting capacitors with sizable energy storage as shown in Figure 1-2. The stretching and compressing of the elastomeric rolls due to the vibration of the wave force provides the power.

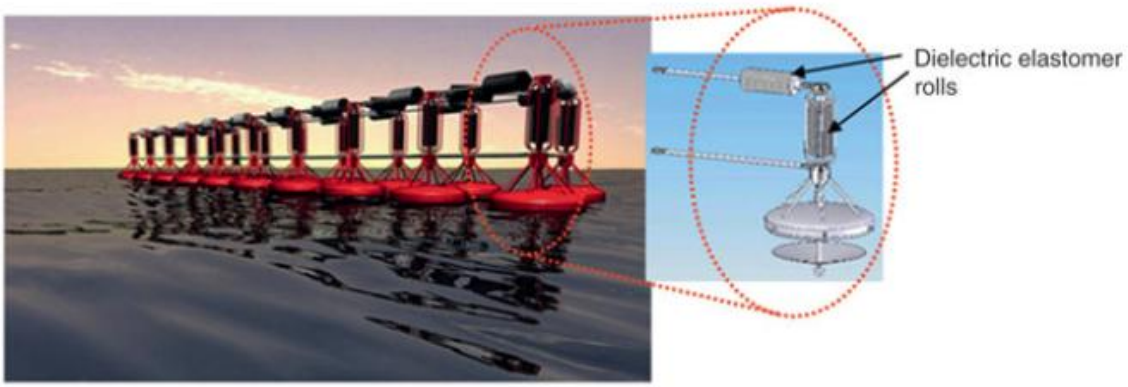

Fig. 1-2 Ocean wave energy harvesting system based on dielectric elastomer transducers.[5]

1-3-2 Braille Displays

Electroactive polymers are an alternative class of materials to piezoelectric materials in enabling cost-efficient refreshable Braille displays. Braille is a standardized six-dot language for visual impaired people to read, write, and communicate. The idea of a responsive and refreshable EAP-based Braille display (shown in Figure 1-3)[6] has been proposed as a new technology that could replace the currently existing Braille technologies, which are expensive and sometimes require complicated printers. In addition, this new refreshable Braille display would be capable of not only showing text but also graphics such as, for example, the graph of a mathematical function. Such a refreshable Braille display would enable visual impaired people to access information more easily including scientific information.

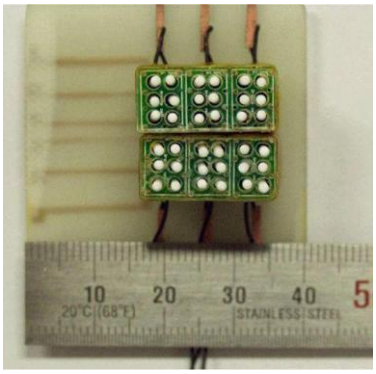

Fig. 1-3 Braille display based on electroactive polymer actuator.[6]

1-4 Summary

Electroactive polymers are a new class of materials that can be employed in power generator and refreshable Braille Display applications because of their low cost, light weight,

and easy manufacturing. They are also attractive because of their elasticity, rapid response, and low power consumption.

In this thesis, the electroactive behavior of one particular kind of polymer is studied that has a low Young's modulus, i.e., a dielectric elastomer. The effect of plain and Janus silica particle fillers on the performance of this dielectric elastomer is investigated. Chapter 2 begins with a brief introduction to the background of dielectric elastomers and their properties. Chapter 3 reviews materials and procedures used, while Chapter 4 provides more details on measurement set ups and techniques employed in this work. A careful analysis of the Young's Modulus and the dielectric constant as a function of filler type and filler amount is presented in Chapters 5 and 6, respectively, which when applied shows that the use of Janus-type fillers enhances the overall electrocactive properties of the dielectric EAP investigated in this thesis (Chapter 7). The thesis concludes with Chapter 8, which provides a summary of the work and gives an outlook on future experiments.

Chapter Two – Background

As discussed in the previous chapter, a quite high E-field (~150 V/m) is needed to generate a significant deformation in an electronic EAP. Upon application of the external electric field, the molecules in the film change their conformation thereby inducing a dipole moment. Based on the morphology, the structure of the polymer, and the relationship between the strain and the applied E-field, electro-mechanical actuation of electronic EAPs is grouped into four types;[1] (i) piezoelectric effect, (ii) electrostriction effect, (iii) Maxwell effect, and (iv) electrets-based effect.

When the deformation is generated due to the piezoelectric effect (i), the relationship between strain and applied E-field is linear. When the deformation is generated by the electrostriction (ii) or Maxwell effect (iii), the strain is proportional to the square of the applied E-field. The deformation generated by the electrets-based effect (iv) involves a much more complicated relationship.[2]

In this thesis, one particular type of electroactive polymer is used, i.e., a Dielectric Elastomer (DE). In a DE, the deformation generated due to electrostatic attraction and the electro-mechanical actuation is best described by the Maxwell effect (iii) discussed in more detail in the following.

2-1 Electromechanical Actuation Mechanism in Dielectric Elastomers (DEs)

The occurrence of the Maxwell stress effect (typical for elastomers) is indicated by a proportional relationship between the observed strain and the square of the applied E-field. The strain caused by the Maxwell stress effect is strongly affected by material defects such as void-

charges and charge-carriers providing an opportunity to enhance the actuation behavior through addition of fillers.

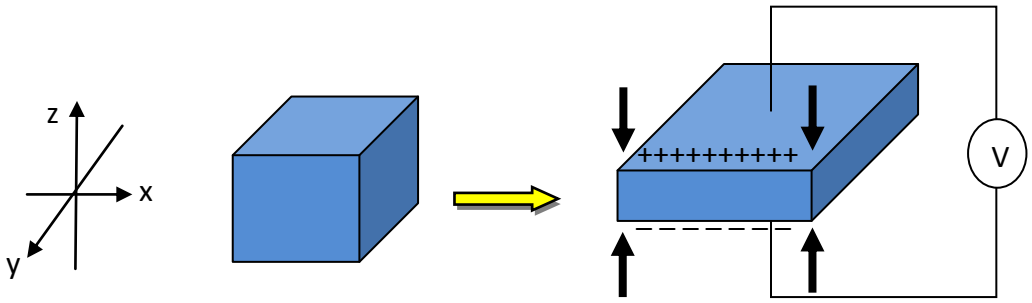

Fig. 2-1 Illustration of Maxwell stress effect in DE.

2-1-1 The Maxwell Effect and Compressive Stress

When dielectric elastomers are exposed to electric fields, opposite charges are induced on the two sides of the elastomer plane as shown in Figure 2-1. The opposite charges attract each other and compress the elastomer due to electrostatic attraction. The compressive stress $(\sigma_z)^3$ experienced by the elastomer is expressed by Eq. 2-1:

$$\sigma_z = \varepsilon_r \varepsilon_o E^2 \qquad (2\text{-}1)$$

Here, ε_o is the dielectric constant of vacuum, ε_r is the dielectric constant of the material, and E is the applied electric field. When the strain is small, we can assume the dielectric elastomer obeys Hooke's law, equation (2-2):

$$\sigma_z = - Y S \qquad (2\text{-}2)$$

in which σ_z is the compressive stress, Y is the Young modulus, also called modulus of elasticity, and S is the strain. Combination of equations (2-1) and (2-2) yields equation (2-3):

$$S_z = -\frac{\varepsilon_r \varepsilon_0 E^2}{Y} \qquad (2\text{-}3)$$

where S_z is the strain along the z-axis. In case of small strains (<20% or within the linear region of the stress-strain curve),[4] equation (2-1) describes the Maxwell stress effect.

The higher the value of strain generated, the more significant is the deformation of the material. Maxwell's equation (2-3) gives insight into possible ways of enhancing the performance of a dielectric elastomer under a fixed electric field. Since ε_o is a constant, we can enhance the strain by either increasing the ε_r value or by decreasing the *Y*-value of the polymer material separately or both at the same time.

2-1-2 Elastic Properties of DEs

The Young's Modulus, *Y*, describes the extension experienced by a material under tension in the elastic region of the stress-strain curve. In other words, a material is much stiffer if it has a high Young's modulus (e.g., Y_{TiO2} ~ 420 MPa vs. Y_{brass} and Y_{bronze} ~ 103-124 MPa)[2]. DEs are typically flexible and ductile polymers with low Young's Moduli, for example, PMMA, has a *Y*-value of 3.2 -3.4 MPa[5] compared to epoxy resins with higher *Y*-values of 2.4 - 5.0 GPa.[6]

Behavior at Large Strains

If the strain is large (> 20%) leading to a non-linear stress-strain behavior, the Young's Modulus, *Y*, becomes a function of the strain. In this case, *Y* has to be treated as a variable. A relationship for DEs has been reported by Yang et al.,[7] equation 2-4:

$$(1+S_x)\,(1+S_y)\,(1+S_z) = 1 \qquad (2\text{-}4)$$

with the condition that the volume of the polymer is constant. This condition is reasonable when the DE is not consumed during or after application of the electric field and the deformations in both the x- and the y-directions are isotropic. A hypothesis that $S_x = S_y = S_{xy}$ has been proposed[8]

leading to a more simplified equation (2-5):

$$S_z = -1 + \frac{1}{(1+S_{xy})^2} \quad (2\text{-}5)$$

Occurrence of Blocking Force and Stress

When the applied E-field is removed, the DE tries to return to its original shape. At the same time, the DE generates a force to restrict this behavior, which is called the blocking force. The blocking force is defined[9] as given in equation (2-6):

$$F_y = \left(\frac{x_o z_o}{\alpha_y}\right) \varepsilon_r \varepsilon_o E^2 \quad (2\text{-}6)$$

with the special condition, that the length in the x-direction is kept constant during the experiment. In Equation (2-6), α_y stands for the displacement in the y-direction, which is equal to y/y_0. The blocking stress, σ_y, is equal to the blocking force, F_y, divided by the cross-sectional area (A_y), i.e., equation (2-7):

$$\sigma_y = \frac{F_y}{A_y} \quad (2\text{-}7)$$

2-1-3 Dielectric Properties of DEs

Dielectric Constant (Permittivity)

The dielectric constant, also called permittivity, is used to describe how a medium interacts with an electric field as well as generates an electric field flux from a charge. Also, it can be used to describe the polarization of a material. However, it is difficult to measure the absolute dielectric constant of a material directly, so usually the relative dielectric constant is used to describe the dielectric behavior in an E-field. The relative dielectric constant, ε_r, is the ratio of

the dielectric constant of a medium relative to the dielectric constant of vacuum.

In this thesis, the task of the fillers added to the DE is to enhance the dielectric constant of the composite (see Chapter 2-1-1). However, it is difficult to measure the dielectric constant of a filler material directly unless it is available as a bulk material. There are reports in which the dielectric constant is derived from comparing the difference of the refractive index of a solution.[10]

An alternative and much more straightforward method is to measure the relative permittivity, ε_r, of the filler material, i.e., the relative dielectric constant. The permittivity is defined as:

$$\varepsilon_r = \frac{\varepsilon}{\varepsilon_o} \tag{2-8}$$

where ε is the dielectric constant of the material, and ε_o is the dielectric constant of vacuum.

Relationship between Dielectric Constant and Capacitance

The capacitance, C_p, describes the ability of a material to store electrical energy, which is used to describe the capacitance, *C*, of an electric capacitor. One coulomb (1 Q) of charge stored per one volt (1 V) leads to one farad (1 F) of capacitance, i.e., $C = Q/V$. The method to measure the capacitance is straight forward. Two parallel conductive layers are prepared to serve as electrodes. The two electrodes of area, *A*, are separated by a fixed distance, *d*, as shown in Figure 2-2. The width of the electrodes is much larger than the separation (*d*) between the two electrodes.

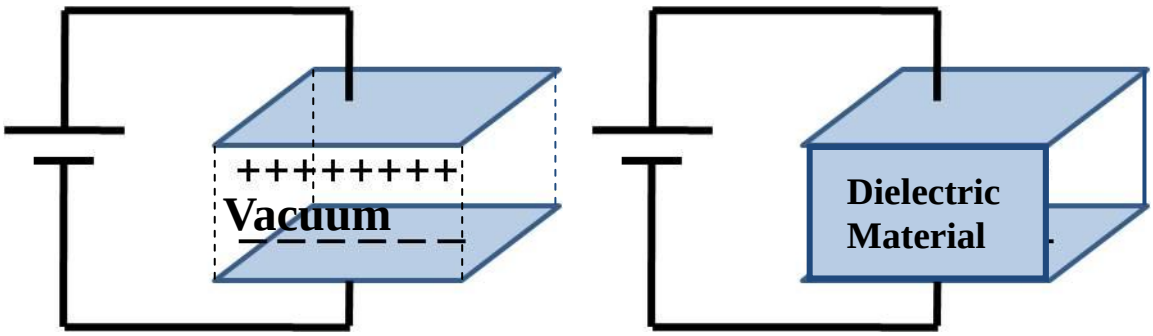

Fig. 2-2 Construction of cell for capacitance test (a) in vacuum and (b) with dielectric material.

When an external voltage is applied to the electrodes, the electrode plates generate an electric field, *E*, between them. The magnitude of the field is:

$$\mathrm{E} = \frac{\rho}{\varepsilon} \tag{2-9}$$

where ρ is the charge density:

$$\pm\rho = \frac{\pm \mathrm{Q}}{\mathrm{A}} \tag{2-10}$$

and $\pm Q$ is the amount of charge, which exists on the surface of the electrodes. The voltage, *V*, between the two electrodes is known through the definition of *V* as the line integral of the electric field, Eq. 2-11:

$$V = \int_0^d E dz = \int_{\varepsilon}^{\rho} dz = \frac{\rho d}{\varepsilon} = \frac{Qd}{\varepsilon A} \tag{2-11}$$

In a DC circuit, the capacitance is defined as:

$$C = \frac{Q}{V} \tag{2-12}$$

which yields:

$$C = \varepsilon \frac{A}{d} \tag{2-13}$$

and

$$\frac{C}{C_o} = \frac{\varepsilon}{\varepsilon_o} = \varepsilon_r \quad (2\text{-}14)$$

for the same capacitor when *A/d* is a constant. Here, *C* and C_o describe the capacitance of the matrix and the vacuum, respectively. The relative dielectric constant of a material, ε_r, can also be obtained from capacitance measurements. In other words, if a material with a high dielectric constant is placed in an electric field, it can introduce a high capacitance into a circuit, which can then be measured.

2-1-4 Classic Young's Modulus and Dielectric Constant Mixing Rule

The theoretical prediction of composite properties is of interest to many research groups and helps us to learn more about the interaction mechanism between fillers and a matrix. In this thesis, mixing theories are used to explain the observed Young's modulus and dielectric constant of the composites and are briefly introduced here.

Young's Modulus Mixing Rule of Composite

In 1906, Einstein proposed a viscosity law for rigid spheres suspend randomly in a liquid, which states that the overall physical properties are effected by the filler concentration, C_f, if the solution is dilute (<10%).[11] For example, the composite viscosity ($<\eta>$) can be expressed as shown in Eq. 2-15[12]

$$<\eta> = \eta_m [1 + 2.5C_f] \quad (2\text{-}15)$$

Further, the characteristic properties of the composite at low filler concentration (< 10%) can be described with a power series linear equation depicted in Eq.2-16

$$<p> = p_m [1 + \alpha 1\ C_f + \alpha 2\ C_f^2 + \alpha 3\ C_f^3 + \dots] \quad (2\text{-}16)$$

For a composite with a high filler concentration (> 10%), the particles are not isolated within the bulk material and start to interact with neighboring particles. In 1945, Guth and Simha[13] introduced a theory that assumed the spherical particles form short chains to develop conducting bridges inside the polymer system when the concentration is higher than 10% but less than 30%. In order to account for this stringing behavior, one more term is added to the original model (Eq. 2-15) in form of a polynomial series expansion shown in Eq. 2-17 where <E> is Young's Modulus of composite:

$$< E > = E_m [1 + 2.5C_f + 14.1 C_f^{\,2}] \quad (2\text{-}17)$$

In 1951, Mooney[14] used a crowding factor, g_f, shown in Eq. 2-18 to fit the theoretical prediction to experimental results.

$$< E > = E_m [1 + 0.67 g_f V_f + 1.62 g_f^{\,2} V_f^{\,2}] \quad (2\text{-}18)$$

For an anisotropic composite, the aspect ratio and orientation of the fillers are very important. There are two different models that describe filler re-enforced polymers with the corresponding properties of the matrix and the fillers based on their proportion and geometry, one is the Halpin-Tsai Equation[15], Eq. 2-19:

$$\text{Er} = \frac{Ec}{Em} = \frac{1+ \xi \bullet \eta \bullet \varphi}{1-\eta \bullet \varphi}$$

$$\eta = \frac{Ef/Em-1}{Ef/Em+\xi}] \quad (2\text{-}19)$$

Here $\xi = 2$ (L/D) is the geometry factor where L/D is the filler's aspect ratio. In the Halpin-Tsai Equation, it is assumed that the fillers are oriented and bonded firmly within the polymer network. For a random dispersion at low concentrations, Schaefer et al.[15] formulated Equation (2-20):

$$\text{Er} = 1 + 2 \left(\frac{L}{D}\right) C_a \varphi \quad (2\text{-}20)$$

in which C_a is an angular factor, which equals to 0.2 and is independent of filler size.

Dielectric Constant of Mixing Rule of Composite

Several models have been derived to describe the dielectric constant of a composite relative to its components – the polymer and the filler. For example, the Kerner equation[15] (2-21), and the Lichtenecker equation[15] (2-23) to name a few.

$$\varepsilon_c = \frac{\varepsilon_1 v_1 + \varepsilon_2 v_2 (E_{2z}/E_{1z})}{v_1 + v_2 (E_{2z}/E_{1z})} \qquad \text{Kerner equation} \qquad (2\text{-}21)$$

whose electric field can be rewritten as:

$$E_{1z} = E_o,\ E_{2z} = \frac{3\varepsilon_1}{2\varepsilon_1 + \varepsilon_2} E_o \qquad (2\text{-}22)$$

$$\ln(\varepsilon_c) = v_1 \ln(\varepsilon_1) + v_2 \ln(\varepsilon_2) \ \text{ with } \ v_1 + v_2 = 1 \qquad \text{Lichtenecker equation} \qquad (2\text{-}23)$$

Here, ε and v are the dielectric constant and the volume fraction, respectively. The indices c, 1, and 2 denote the composite, material 1 (matrix), and material 2 (filler), respectively. To enhance the overall dipole moment or dielectric constant of a DE, some groups[16] have added specifically structured filler material, such as core-shell nanoparticles. Furthermore, the Kerner Model[15] has been modified to fit the three components of such a composite, Eq. (2-24) to (2-26). Here, α is the impact factor, which is based on the structure of the filler material.

$$\varepsilon_{eff} = \epsilon_1 + v_2(\varepsilon_2 - \varepsilon_1)a_2 + v_3(\varepsilon_3 - \varepsilon_1)a_3 \qquad (2\text{-}24)$$

$$a_i = 1 - \frac{1}{3}\left[(\varepsilon_i - \varepsilon_{eff})^{-1}\varepsilon_{eff} + \frac{1}{3}\right]^{-1} \qquad i = 2,3 \qquad (2\text{-}25)$$

$$\sum_{i=1}^{3} f_i a_i = 1 \qquad (2\text{-}26)$$

From the above equations, it is possible to estimate the dielectric constant of a composite and compare it to the number calculated from the Maxwell Equation fitted to the stress-strain response obtained from the electric field test of the actuating films.

2-1-5 Overall Electro-Mechanic Efficiency (K^2)

Due to energy conservation, the output elastic energy density of a dielectric elastomer actuator should be always less than its input elastic energy density.[17] Therefore, the coupling between input and output elastic energy is a criterion by which to judge the electro-mechanic efficiency of an actuator.

Output Elastic Energy Density

The output elastic energy, E_S, can be defined as the integral compressive force applied to the surface of a specimen over the displacement in the z-direction, which can be written as shown in Eq. 2-27

$$E_S = \frac{-\sigma_M S_z}{2} \tag{2-27}$$

Here, we assume the electrostatic stress (σ_M), i.e., the compressive stress (σ_z) in Eq. 2-1, is constant and equal to ($-YS_Z$), which is fulfilled when the strain is less than 10%. Thus,

$$E_S = \frac{YS_Z^2}{2} \tag{2-28}$$

If the strain is much larger than 10%, we make the same assumption as before that the volume is constant and the deformations in both x- and y-directions are isotropic. The corresponding stored elastic energy, E_L, can then be rewritten as depicted in Eq. 2-29:[3]

$$E_L = -\sigma_M \ln(1+S_Z) \tag{2-29}$$

where Pelrine et al. assume that electromechanical force is constant and the deformation of DEs is isochoric so the area is proportional to strain, $A_z = x_o y_o/(1+S_z)$.[3]

Overall Efficiency[3]

The overall efficiency of actuation, η_t, is defined as:

$$\eta_t = \eta_c \eta_m \eta_d \tag{2-30}$$

where η_c is the electrical efficiency, η_m is the mechanical efficiency, and η_d is the electric driver circuit efficiency. Here, the electric driver circuit efficiency refers to the electrical energy converted into mechanical work, which can be calculated dividing the stored mechanical energy by the input electrical energy under the assumption that the input electrical energy equals the work output by the power supply. η_d is a function of K^2, where K^2 is the electromechanical coupling efficiency, which can be calculated as given in equation (2-31).

$$K^2 = - 2 S_z - S_z^2 \quad (2\text{-}31)$$

The K^2 values of commonly used DEs are listed in the Table 2-1. The high K^2 value of elastomers such as acrylic and silicone are preferred for actuators. In the next section, we will focus on the comparison of various types of ealstomers.

TABLE 2-1 Electromechanical coupling efficiency for various elastomers.[8]

Elastomers	K^2
Acrylic	50 – 90
Silicon	60 – 70
Fluorosilicone	48
Polyurethane	21

2-2 Dielectric Elastomer Composites

2-2-1 Dielectric Elastomers (DEs)

The applicability of dielectric elastomers as electroactive polymers was recognized in the 1990s. Their high elasticity and high dielectric constant promise better performance in

electromechanical applications. Actuation strains larger than 200% have been reported with energy densities as high as 3.4 MJ/m^3, resulting in an electromechanical coupling efficiency larger than 90%.[8]

2-2-2 Physical Properties of DEs

There are a few types of DEs, such as acrylic[18] or silicone elastomers currently under investigation in several research groups. Since the response of DEs is dominated by the Maxwell effect, a dielectric elastomer with low Y and high ε is of interest to fabricate a high strain response actuator. The Y and ε values of common DEs are listed in Table 2-2. Compared to most of the dielectric elastomers, whose ε/Y values range from 0.5 to 7.7, the acrylic elastomer has the highest inherent ratio of ε/Y = 9.6, which makes it suitable for employment in actuators.

TABLE 2-2 Dielectric constant and Young's Modulus of elastomers.[8]

Elastomers	Dielectric constant (ε) [@ 1 Hz]	Young's Modulus (Y) [MPa]	ε/Y [@ 1 Hz]
Fluoroelastomer	13	2.5	5.20
Polyurethane	7.0	17	0.42
Acrylic	4.8	0.5	9.6
Polybutadiene	4.0	1.7	2.35
Silicone	3.3-3.7	0.35- 0.56	7.69
Polyisoprene	2.7	0.85	3.18

2-2-3 Composite of Dielectric Elastomers (DEs) and Fillers

DEs are potentially interesting materials for actuator application. However, their limitation is that most of them have a low R-value (ε/Y - ratio), which means that it is difficult to generate a large shape change with a low voltage. To address this problem, we proposed to load particles with a high dielectric constant into our DE, while at the same time trying to maintain the

characteristics of the DE with respect to flexibility and light weight.

Enhanced Dielectric Elastomer Composites

Recent reports have shown that adding fillers with a high dielectric constant helps to enhance the dielectric constant of a dielectric polymer composite. In 2002, Zhang et al.[19] used a copper-phthalocyanine (CuPc) oligomer as filler and observed a 1.7 times higher strain response of the composite compared to the response of the pure polymer. The authors argue that the CuPc additive helps because its relative dielectric constant, ε_r, is larger than 106. A loading of 40 wt% of CuPc into the matrix of P(VDF-TrFE) successfully enhanced the ε_r value of the material from 40 to 225. In a related study, Huang et al.[20] used polyaniline (PANi) to enhance the transverse strain response of poly(vinylidene fluoride-trifluoroethylene-chlorotrifluoroethylene, p(VDF-TrFE) to 1.5% in a field of 9.5 V/μm, which is an order of magnitude lower than fields used for traditional DE-based actuators in 2003.

However, since the incompatibility of inorganic fillers in organic polymers decreases the breakdown voltage and increases the dielectric loss, researches have also looked for new filler materials with high dielectric constants and low dielectric losses. In 2006, Gilbert et al. measured the dielectric constant of a composite filled with 25% $BaTiO_3$ (BT) powder to be 13 with a dielectric loss of only 0.18.[21] Dang et al. in 2009 reported a dielectric constant of a polyimide composite with 40 vol% calcium copper titanate (CCTO) as 49 @ 100 Hz which is 14 times larger than that of pure polyimide with a dielectric loss of less than 0.2.[22]

Inspired by these recent results, we have investigated the use of gold-coated SiO_2 Janus particles as fillers (see Chapter 2-3).

2-2-4 Dipole Moment

There are three types of dipole moments; (i) permanent dipoles, (ii) instantaneous dipoles, and (iii) induced dipoles. Permanent dipoles occur when two chemically different atoms exhibit a variation in the electron concentration due to the specific interaction between the two atoms. Instantaneous dipoles are temporary dipoles, which are caused by a non-uniform concentration of electrons. An induced dipole is also a temporary dipole, but is induced by the approach of a permanent dipole or an external electric field.

For example, both hydrogen fluoride (HF) and water (H_2O) molecules have a non-uniform charge distribution between their atoms and as a result exhibit a strong permanent dipole moment with an inherent electric field. The dipole moment is a parameter to indicate the polarity of a molecule or object. The strength of the dipole moment is proportional to the dielectric constant and the length of the dipole.

2-3 Janus Particles

Janus is an ancient Roman God with two faces on opposite sides. For the purpose of this thesis, silica particles are coated with gold on one hemisphere. These gold–capped silica particles are called Janus particles because of their anisotropic surface with differing chemical or physical properties[23] where one side is metal-like and the other is oxide-like in analogy to the Janus god with his two distinguishable faces.

Janus particles were first mentioned in the literature by Casagrande et al.[24] and then showcased in de Gennes' Nobel Lecture[25]. In 1997, Takei et al.[26] observed the orientation of Janus particles in low frequency (0.1~1 Hz) electric fields. Later, Crowley et al.[27] reported on the "gyricon" ball, a polymer particle with two polymer compartments with different electrical

properties resulting in a dipole response, which was used as E-ink in electronic paper in 2002. Gangwal et al.[28] in 2008 focus on the electrophoresis behavior of Janus particles which experience induced charge on one side. They also found that the particles can be assembled in AC electric field with frequencies ranging from 100 to 10kHz.[29] These experimental findings justify the expectation that if the two halves of a Janus particle vary greatly in their physical properties, a high dipole moment is expected. Thus, addition of Janus particles as filler material to a DE is expected to enhance the dielectric constant compared to the pure DE. In addition, the Janus structure provides a means for introduction of non-planar metal pieces and a more uniform distribution of these metal pieces in the polymer matrix.

2-4 Summary

Dielectric elastomers represent a suitable material for application in actuators. Addition of high dielectric fillers to the dielectric elastomers is expected to enhance the overall dielectric constant of the composite, while not affecting the flexibility of the dielectric elastomer. The choices of the added filler amounts, the dispersion in the matrix, and the structure of the fillers are important factors that affect the eletromechanical performance of the resulting dielectric elastomer composite actuators and will be studied in this thesis.

Chapter Three – Materials & Synthesis

In this chapter, the materials and synthesis methods used to prepare the dielectric elastomer, fillers, and actuator films employed throughout the thesis for studying the mechanism of electro-mechanical actuation of plain, SiO_2, and Janus particle SiO_2 filled actuator films are introduced.

3-1 Bulk Material

Acrylic polymers, also called acrylates, are used by many researchers in the field of actuation because of their transparency, resistance to breakage, and high elasticity.[1] However, for DEs to be successfully employed in high field actuation they are required to be flexible materials with high dielectric constants to induce a high strain response at a reasonably low applied field. The combination of flexibility and high dielectric constant, i.e., strong dipole moment, is problematic because strong dipoles lead to strong intermolecular interactions and increased material stiffness. Separation of the Young's Modulus and the dielectric constant properties through use of fillers with high dielectric constants has been proposed as an approach to enhance the overall dielectric constant of DEs without sacrificing the DEs' flexibility. In the following, the physical properties of the monomer - ethylene glycol phenyl ether acrylate (EGPEA) - and the preparation of the precursor mixture will be discussed.

3-1-1 Ethylene Glycol Phenyl Ether Acrylate (EGPEA)

Ethylene glycol phenyl ether acrylate, EGPEA, is our target monomer. Its structure is shown in Fig. 3-1 (a). During the polymerization period, the double bond at the top end of the molecular structure in Fig. 3-1(a) opens and monomers link to other EGPEA monomers (Fig. 3-1 (b)) through radical polymerization. Acrylate-type polymers have a high polarity because of the big polar ethyl phenyl ether side group in their monomer unit.

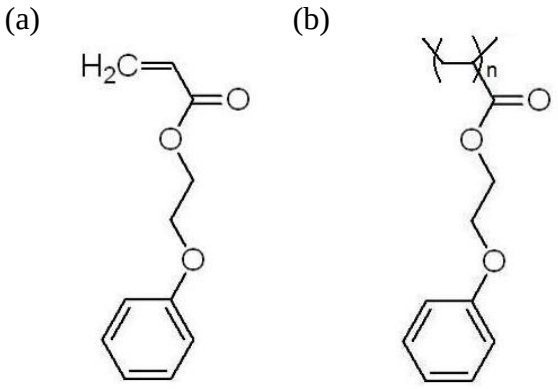

Fig. 3-1 (a) Molecular structure of EGPEA monomer. (b) Molecular structure of repeat unit in p(EGPEA).

Glass Transition Temperature, T_g

The glass transition temperature, T_g, is the temperature at which a material changes from a glassy state to a rubbery state. T_g is a very important parameter in actuation materials because when the operating temperature decreases below T_g, the polymer will become brittle and unusable for actuation. When the polymer is heated above T_g, it is soft and elastic. Due to the low transition temperature of p(EGPEA) (T_g= -36^{o}C), p(EGPEA) is able to maintain its low Young's Modulus during operation at room temperature.

Influence of Monomer Structure

A second advantage of the EGPEA monomer is its phenyl-ring structure. The phenyl ring helps to keep the polymer chains separated due to the group's bulkiness increasing the elasticity of the p(EGPEA) polymer. Another way to improve the elasticity of a polymer is the addition of a copolymer to construct sections with different properties. Generally, these copolymers are comprised of blocks formed by macromolecules that generate regions for contraction and expansion.

3-1-2 Preparation of Bulk Material Precursor Mixture

The bulk material, Ethylene glycol phenyl ether acrylate (EGPEA), is purchased from Sigma-Aldrich containing 100 ppm of hydroquinone as inhibitor. To obtain pure EGPEA monomer, the inhibitor is removed by passage through a pre-packed inhibitor remover column packed with Al_2O_3 powder (Sigma-Aldrich). 2000 μL of the pure EGPEA monomer fluid are then mixed with 70 μL of the crosslinker, 1,6-hexanediol diacrylate, in a molar ratio of 97:3. The crosslinker is also purchased from Sigma-Aldrich (80%, inhibited with 100 ppm of methyl ether hydroquinone) and inhibitor-cleaned using the same type of packed column. Next, 17 mg of 2-benzyl-2-(dimethylamino)-4'-morpholinobutyrophenone, obtained from Sigma-Aldrich (97%) are added to serve as the photoinitiator during UV curing of the liquid precursor mixture. The weight ratio of monomer, crosslinker, and photoinitiator in the precursor mixture is 96:3:1.

3-2 Filler Materials

Two types of filler materials have been studied in this thesis work; (i) surface-isotropic 500 nm silica particles (SiO_2) and (ii) surface-anisotropic 500 nm gold-capped silica Janus particles (JP SiO_2).

3-2-1 Silica Particles

500 nm diameter, monodisperse silica spheres (<10% size distribution) were purchased from Angstrom Sphere and used as received. The unmodified silica spheres exhibit hydrophilic surface properties in aqueous electrolyte due to their negative zeta potential.[2] The negative charges are responsive to an electric field. The silica particles are tested as fillers in order to distinguish the effect of the silica filler material on the p(EGPEA) properties from those caused by the surface-anisotropic JP SiO_2 particles.

3-2-2 Silica Janus Particles

Silica Janus particles are silica particles that have been partially surface modified with a metallic cap. These modified particles carry a high local dipole moment due to their discontinuous surface charge. They are manufactured in three steps; (i) convective assembly of silica spheres, (ii) metal vapor deposition of the metal cap, and (iii) re-suspension of the JP SiO_2 particles.

Convective Assembly

First, two acid-treated glass slides are brought into contact with each other at an angle θ. Then, a small amount (5 μL) of concentrated silica particle suspension (30 wt %) is inserted

between the wedge formed by the two slides (Figure 3-2 (a)). A syringe pump is used to drag or push the upper glass slide across the stationary bottom glass slide at room temperature and in controlled humidity. As the liquid evaporates, the convective forces between the spheres lead to an ordered, close-packed monolayer on the surface of the bottom glass slide as shown schematically in Figure 3-2 (b).

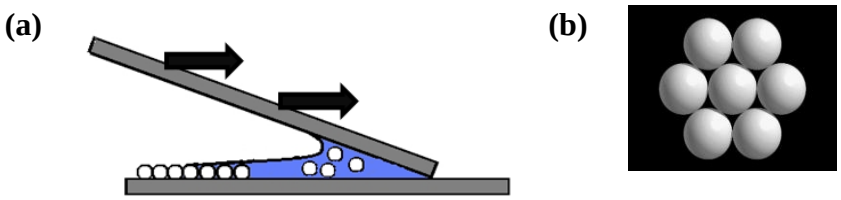

Fig. 3-2 (a) Schematic of convective assembly method. (b) Closed-packed structure of particle monolayer.

Physical Vapor Deposition

The hemisphere of each silica particle in the monolayer is modified by physical vapor deposition (CRESSINGTON coating system, 308R). This PVD machine has two sources and thus two materials can be evaporated without opening the chamber. Two layers are evaporated onto the particles; a 5 nm layer of titanium followed by a gold layer of 20 nm (Figure 3-3 (a)). The Ti layer serves to enhance adhesion between the silica surface and the gold cap. The resulting particles exhibit distinct surface portions; one half is silicon dioxide and the other half is metallic gold, i.e., a Janus particle structure (see Chapter 2-3). Particles with this surface morphology (Figure 3-3 (b)) break the balance of the original charge distribution and are believed to act more like bipolar particles.[3] They will move or assemble into well-defined

clusters according to their charge, charge distribution, and the strength and direction of the electric field they are exposed to.

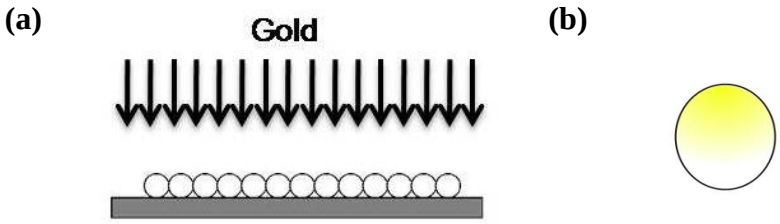

Fig. 3-3 (a) Schematic of metal deposition (PVD) process. (b) A Janus particle – yellow color indicates gold and white color indicates SiO_2 portion.

Sonication

After surface modification, the Janus particle layers are sonicated off the glass slides into deionized water and dried in an oven at ~ 22 ℃ leading to a dry powder of Janus particles.

3-3 Fabrication of Composite Films

Three steps are necessary to obtain p(EGPEA) actuator films. First, the filler has to be mixed thoroughly with the EGPEA precursor mixture. Then, the precursor mixture has to be cast into a mold that shapes it into the desired film geometry. Last but not least, the precursor mixture needs to be photo-polymerized. The process is described in the following for the case of p(EGPEA) with Janus particle fillers, but an identical procedure is employed for p(EGPEA) with silica particle fillers and the pure p(EGPEA) films.

3-3-1 Preparation of PDMS Soft Stamp Replica Mold

Poly(dimethylsiloxane), PDMS, is widely employed in microfluidics and other applications.[4] Because it is cheap, flexible, easily-processed, and chemical inert due to its stable alkyl side groups,[4] we use it as our replica mold.

The liquid mixture of the PDMS base and agent (weight ratio of 10:1) is poured onto the surface of a glass slide. The glass slide with the liquid PDMS mixture is exposed to vacuum for about 20 minutes to remove bubbles in the liquid PDMS. If a few small bubbles remain inside the PDMS pre-polymer liquid after vacuuming, the desiccator is vented more slowly. The bubbles usually shrink and disappear when the desiccator has returned to atmospheric pressure. Then, the PDMS is cured on the heater at 80 ℃ for 25 min. Before the liquid PDMS mixture is completely cured, another clean glass slide is placed gently on top to create a PDMS film with two smooth surfaces. Next, the PDMS mold is peeled off from the glass slide. The resulting PDMS mold is a transparent and flexible material, which allows easy separation of the p(EGPEA) film from the PDMS mold.

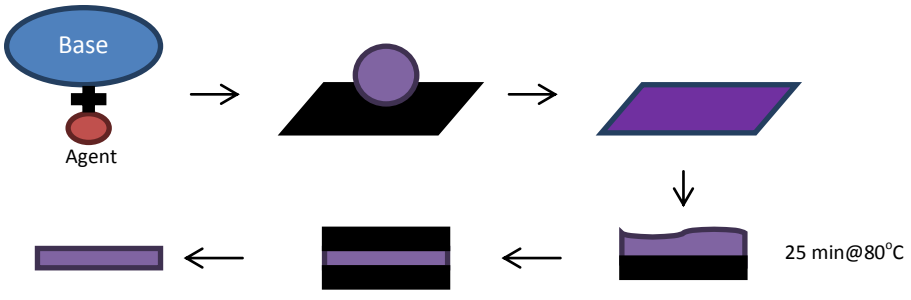

Fig. 3-4 Schematic of soft PDMS replica mold preparation.

3-3-2 Mixing of Filler and the DE Matrix

A 0.5 vol% mixture of dry Janus particle powder and precursor solution is prepared by thoroughly mixing the two components. Note a low loading of Janus particles (0.5 vol%) is used due to the limitations of currently available Janus particle production methods (> 5mg per batch). Then, 40 μL of the well-stirred filler particles/EGPEA precursor mixture are placed on the conducting side of an FTO-glass piece (1x1 $inch^2$). The mixture spreads across the FTO upon covering with the flat transparent PDMS mold.[5] The PDMS mold, precursor mixture, and FTO-glass are assembled into a sandwich structure for curing yielding films with thicknesses ranging from 30 - 60 μm.

3-3-3 Photo-Polymerization

Subsequently, this sandwich structure is placed under a UV Lamp (Spectroline SB-100P, 365nm) for 13 min to initiate polymerization of the precursor mixture. During this process the cell is placed such that the side with the PDMS mold faces up towards the UV lamp. The distance between the film and lamp is ~5 cm. After removal of the sandwich from the UV Lamp, it is left on the bench to cool down. The EGPEA usually adheres more strongly to the FTO glass. The elasticity of the PDMS mold enables its easy removal yielding thin JP SiO_2-p(EGPEA) films with thicknesses ranging from 30 - 60 μm on the conducting side of the FTO glass slide. An illustration of the 3D structure of the entire JP SiO_2-p(EGPEA) film and its cross-section indicating a uniform JP SiO_2 dispersion are shown in Fig. 3-5. A similar procedure is employed for preparation of the films with SiO_2 particles as fillers and the pure p(EGPEA) polymer films.

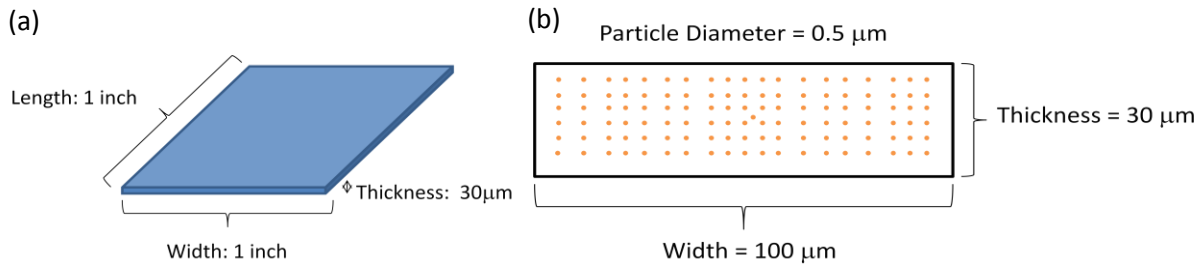

Fig. 3-5(a) Illustration of the 3D structure of the JP SiO_2-p(EGPEA) film. (b) Illustration of uniform dispersion of 0.5 vol% JP SiO_2 within the polymer film in cross-sectional view.

3-4 Summary

Materials used and the preparation of p(EGPEA) films for Young's Modulus, capacitance, and actuation measurements are described. A 96:3:1 mixture of EGPEA monomer, 1,6-hexanediol diacrylate (cross linker), and photoinitiater is used to prepare pure p(EGPEA) films and films with unmodified and modified silica particle fillers using a PDMS soft molding technique. Silica particles with Janus structure are prepared by a combination of monolayer assembly and metal evaporation. Subsequently, these films are used to characterize the behavior of the elastomer as a function of the two filler materials during actuation of the films. Depending on the characterization methods, the filler-injected composites are made into various shapes and structures as discussed in the next chapter.

Chapter Four - Characterization Methods

As mentioned previously, the goal of this thesis is to study the effect of Janus particles on the electromechanical properties of p(EGPEA) films. To characterize the effect of Janus particle fillers on the actuation behavior of the composite films, three properties of the p(EGPEA) composite need to be monitored; (i) the Young's Modulus, (ii) the dielectric constant, and (iii) the electromechanical actuation mechanism. In addition, measurements used to determine the physical properties of the fillers, the elastomers, and the composite films are also reviewed here.

4-1 Physical Characterization of the Filler, p(EGPEA), and the Composites

This section reviews the analytical techniques used to characterize the physical properties of the filler, the p(EGPEA) films, and the composites; (i) Scanning Electron Microscopy (SEM), (ii) Thermogravimetric Analysis (TGA), (iii) Atomic Force Microscopy (AFM), and (iv) Optical Microscopy.

4-1-1 Scanning Electron Microscopy (SEM)[1]

SEM is employed to study the surface properties of materials in the micron to nanometer range. For example, it is used to study the morphology of particles such as their shape, size, and their arrangement within a material. In this thesis, an SEM (Zeiss EVO 40) is used to determine the structure of the unmodified and the gold-capped Janus particle fillers and their dispersion within the thin film composites (film thickness: 30 - 60 μm).

Theory of Operation

An SEM operates similar to an optical microscope. The difference is that instead of a light source the SEM uses electrons, which allow for a resolution in the 1 - 20 nm range depending on the specific instrument used. Theoretically, the best resolution of a microscope can be derived from the distance (d) related to the wavelength (λ) of the light used according to Abbe's Law:

$$d = \frac{0.612\lambda}{n \sin \alpha} \tag{4-1}$$

where $n \sin\alpha$ is equal to NA standing for the numerical aperture of the system. The wavelength of visible light is 400 – 700 nm, while that of an electron is only 6 pm.

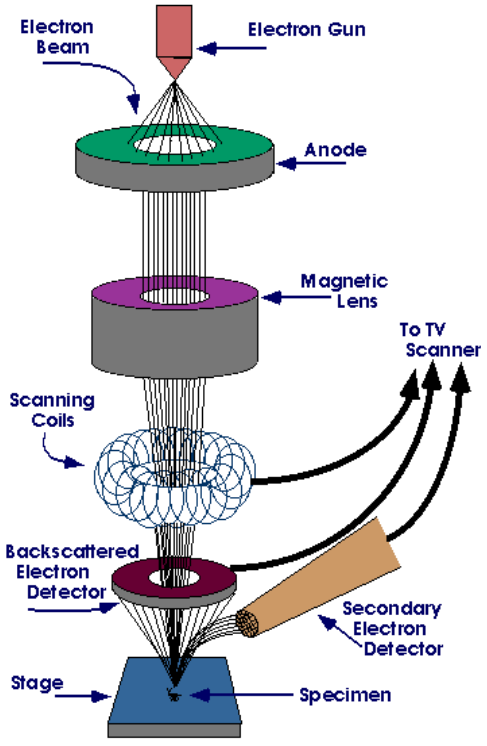

Fig. 4-1 Configuration of an SEM.[1]

In the SEM, the electrons pass through a vacuum column and are focused by electromagnetic lenses as schematically depicted in Figure 4-1. Final, the electron beam hits the sample and

secondary electrons are generated, which are collected by a detector with a photomultiplier. Depending on the electron density of the material interacting with the primary electron beam more or fewer secondary electrons are generated. For example, gold has a higher electron density than, for example, carbon and therefore yields a larger number of secondary electrons giving a higher signal, i.e., resulting in a brighter image. For conventional imaging in the SEM, specimens must be electrically conductive, at least at the surface, and electrically grounded to prevent the accumulation of electrostatic charge at the sample surface.

4-1-2 Thermogravimetric Analysis (TGA)[2]

Thermogravimetric Analysis (TGA) is a method that gives information about the composition and the thermal stability of a material. It records the weight loss as a function of time under application of a constant heat flux. The temperature of the sample is increased gradually and the weight is monitored. Materials with lower boiling points or decomposition temperatures will evaporate/decompose first.

Theory of Operation

Figure 4-2 shows an exemplary TGA measurement of N,N-bis-(1-naphyl)-N,N-diphenyl-1,1'-biphenyl-4,4"-diamine.[3] The graph shows the weight as a function of temperature. Initially, the curve is flat. Then, near 350 ℃ the curve drops quickly indicating removal of material from the sample. Extending the lines from the linear portions of the graph, an intersection of the two lines is found at ~486 ^{o}C, which is the degradation temperature of the polymer. Note, sometimes large weight losses are observed near 100 ^{o}C because of the evaporation of water due to moisture absorbed by the polymer. This feature of TGA can be employed to also measure the water content in a polymer.

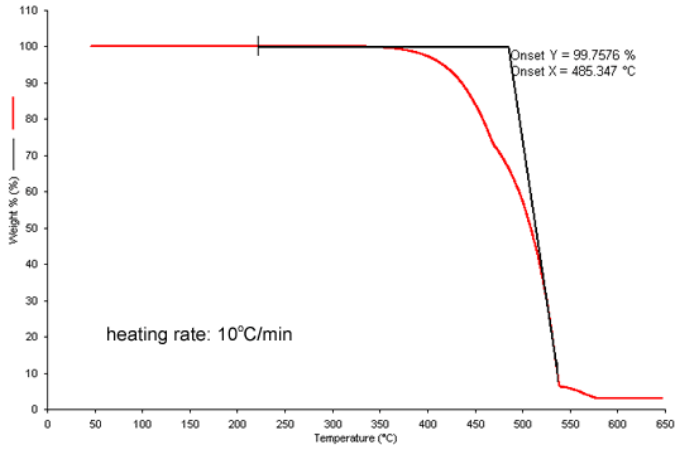

Fig. 4-2 Determination of decomposition temperature of N,N-bis-(1-naphyl)-N,N-diphenyl-1,1'-biphenyl-4,4"-diamine with TGA.[3]

4-1-3 Atomic Force Microscopy (AFM)[4]

AFM is a technique used to measure the surface topology of materials. There are three main modes of AFM; contact, tapping, and non-contact. In this thesis, the tapping mode is used, in which a cantilever taps the surface of a sample and the attractive forces between atoms of the sample and the cantilever tip controlled by an AC voltage are measured. This mode is appropriate for DEs because they are very soft and sticky. In tapping mode, the cantilever uses a smaller force and does not stay in contact with the surface compared to contact mode leading to less damage of the sample surface.

Theory of Operation

An AFM consists of a laser source, a photodiode, and a cantilever with a tiny probe tip used to touch the surface. Different properties of the surface investigated require specialized tips

that can measure all types of forces such as van der Waals force, mechanical contact force, electrostatic force, capillary force, magnetic force, etc. The AFM uses a position sensitive detector, i.e., a photodiode, to collect the laser beam reflected of the back of the cantilever used to scan the surface. The shift of the beam caused by the movement of the tip due to interactions with the surface is plotted as a function of the cantilever position. The set-up is shown schematically in Figure 4-3.

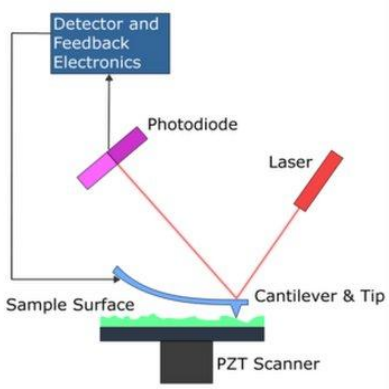

Fig. 4-3 Configuration of the AFM.[4]

4-2 Characterization of the Young's Modulus[5]

To determine the Young's Modulus difference between pure, SiO_2-loaded, and JP SiO_2-loaded p(EGPEA) films, two analytical techniques are used; one is the mechanical analyzer for macroscopic tensile tests and the other one is nanoindentation for microscopic compression tests.

4-2-1 Tensile Test

Mechanical properties such as the Young's Modulus and the tensile stress of a material are determined using a stress-strain experiment performed by a mechanical analyzer as sketched in

Figure 4-4.

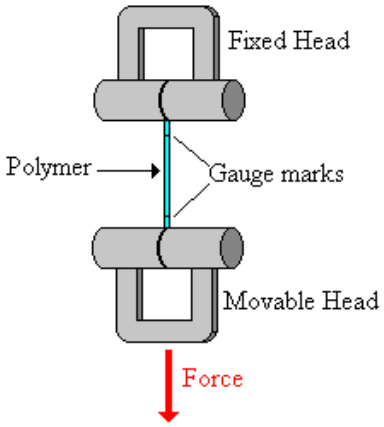

Fig. 4-4 Schematic of setup for stress-strain experiment.[5]

In Figure 4-4, the two ends of a specimen are connected to the two clamps of a tensile tester. The top clamp is fixed and a force is applied by pulling the bottom clamp. The applied force is recorded as a function of sample elongation as shown in Figure 4-5. Two sets of information are obtained from a stress-strain curve, the Young's Modulus, *Y,* and the tensile strength, σ_t.

Young's Modulus of Elasticity

As mentioned in Chapter 2-1-1, the Maxwell effect is a measure of the flexibility of a material. Using Hooke's law, equation 2-2, it is clear that the stress is linearly proportional to the applied strain. The Young's Modulus is determined from the slope of the linear region of a stress-strain curve as shown in Figure 4-5.

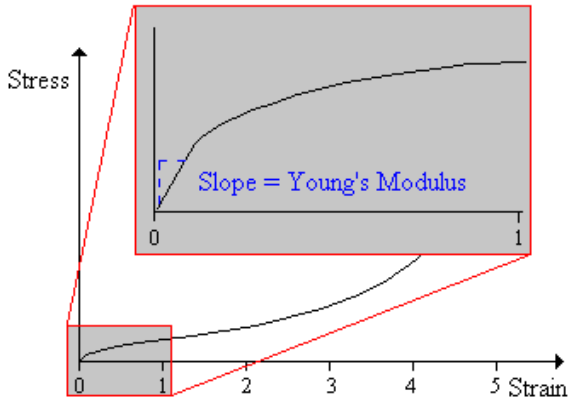

Fig. 4-5 Determination of Young's Modulus from the result of stress-strain experiment.[5]

Tensile Strength

The end point of a stress-strain diagram for a polymer, i.e., the breaking point, describes the strength needed to rupture the polymer and is called the tensile stress of a polymer, σ_t.

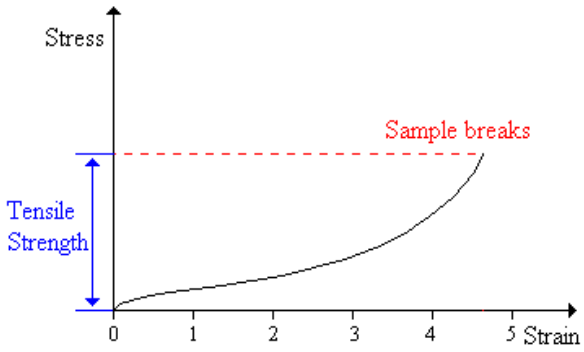

Fig. 4-6 Determination of the tensile stress of a polymer form the result of a stress-strain experiment.[5]

4-2-2 Compression Test

In Chapter 2-1-1, the Maxwell effect was discussed with respect to the compressive strain along the direction of the E-field induced by the application of an external E-field. In a

compression measurement, a nanoindenter is used to measure the mechanical properties of a very thin and small volume of sample. By comparison, the resolution of thevmechanical analyzer is not as good as that of a nanoidenter.

Theory of Nanoindentation[6]

The equipment set-up of a nanoindenter is shown schematically in Figure 4-7. The nanoindenter consist of the indenter tip, the capacitance displacement gage, the magnet, the coil, and the spring. The movement of the tip is controlled by the electromagnetic force. There are numerous available tip geometries such as three and four sided pyramids, wedges, cones, cylinders, filaments, and spheres.

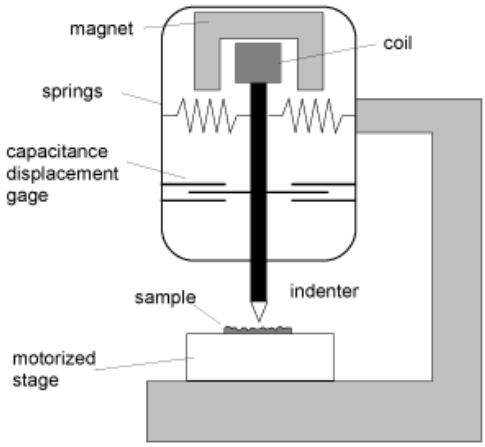

Fig. 4-7 Schematic representation of a nanoindenter.[7]

Due to the small contact surface, the tip geometry is very important. Two well-established common standards are the Berkovich and the cube corner nanoindenters.[8] Compared to the traditional analysis of the Young's Modulus from the stress-strain curve (see above), the nanoindenter uses the force from the force-displacement curve (shown in Figure 4-8), which is used to determine elasticity, hardness, yield strength, and wear properties of materials.

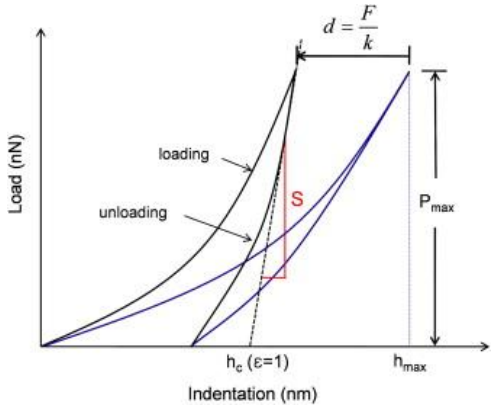

Fig. 4-8 Schematic of a load vs. displacement curve obtained from a nanoindentation compression test.[8]

4-3 Measurement of the Dielectric Properties of a Material[9]

To determine dielectric properties such as permittivity or dielectric loss of pure p(EGPEA), SiO_2, and JP SiO_2-loaded p(EGPEA) thin films, a capacitor cell with two electrodes as drawn in Figure 2-2 is employed. The capacitor cell is filled with the pure or composite p(EGPEA) material. A voltmeter is used to measure the voltage drop across the capacitor cell while the electrodes are charged. Dividing the amount of the charge applied by the measured voltage drop yields the capacitance of the material between the two electrodes. Comparison of the capacitance of the material measured to that of the same cell with vacuum between the electrodes yields the permittivity of the material, as shown in Eq. 2-14.

Theory of Frequency-Dependent Dielectric Constant

Generally, the dielectric constant of a material increases proportionally to the polarization of the material caused by the applied E-field. Polarization of the material includes ionic, orientation of polar groups, and electronic or atomic responses caused by the external E-field. Electronic or atomic responses contribute to the dielectric constant at high frequency; while ionic

responses or responses due to the orientation of polar groups contribute to the dielectric constant in the low-frequency regime as shown in Fig. 4-9.

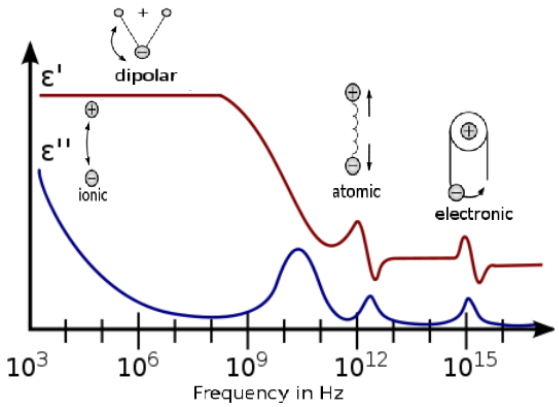

Fig. 4-9 Frequency dependent permittivity and dielectric loss.[10]

Capacitance Measurement Set-Up

A probe station (shown in Fig. 4-10) connected to a HP4284A LCR meter is used to measure the capacitance and dielectric properties of the polymer films tested in this thesis in the range from 20 Hz to 2 MHz. The capacitance of the films is determined and then used in conjunction with the films thicknesses (30 - 60 μm), the electrode cross sectional projected areas (134 - 139 mm^2), and the permittivity of vacuum (8.854 x 10^{-12} F/m), ε_0, to calculate the relative dielectric constants of the polymer films, ε_r.

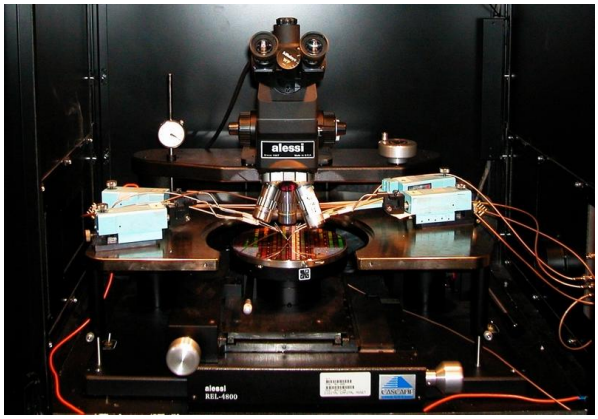

Fig. 4-10 Probe station used for capacitance measurements.[11]

4-4 Electroactive Actuation Test of the Composite Films

The compressive strain experienced by a material is related to the E-field induced by the voltage. This phenomenon is called the Maxwell effect. To determine the Maxwell effect for a particular material, we need to measure the strain of the material under a well-defined E-field. Due to the flexibility of the p(EGPEA), the optical surface profiler is a good, non-contact method to measure any changes in thickness.

Theory of Surface Profiler[12]

This study uses the WYKO NT 1100 to measure the actuation performance of the DE films under electrical stimulation. Generally, the optical surface profiler consists of a light source, a detector, and a computer to image and analyze the data. For the WYKO NT1100, a tungsten halogen lamp projects filtered light from a white-light source (centered at 632 nm) to generate interferences fringes. After the interferometry set up has captured the fringe, the Wyko vision® software is used to analyze the optical signal and to convert it into data that allows the reconstruction of a 2D/3D map of the measured surface. The limitation of the surface profiler for the step height is 5 mm with an accuracy of around 10 - 30 nm. The transverse solution is affected by the aperture of the objective and the magnification of the field of view (FOV). If the material used is transparent or unreflective, a reflective coating needs to be applied on the top side of the sample. To improve the accuracy of our measurements, the piece of Si-wafer is coated with a thin gold film.

4-5 Summary

Analytical techniques used for the determination of the physical properties of the filler materials, polymer films, and composite films are reviewed. Further, measurement techniques are described that enable the determination of the mechanical properties, the dielectric properties, and the electromechanical behavior of the pure and filled p(EGPEA) films, which are three important properties that need to be monitored to elucidate the effect of Janus particles on the actuation properties of p(EGPEA).

Chapter Five – Elastic Property of Pure and Composite p(EGPEA) Films

5-1 Introduction

Dielectric elastomers (DEs), whose electromechanical performance is best described by the Maxwell equation (Eq. 2-3), are good candidate materials for artificial muscles or energy harvesting due to their appropriate dielectric constant and low Young's Modulus compared to many other types of either electronic or ionic electroactive polymers. However, their low electric breakdown strength has so far limited their practical application. To overcome this problem, it has been proposed that the addition of a high dielectric filler material such as metal-oxide[1] or carbon black[2] should lead to an enhancement of the overall dielectric constants. However, the injection of filler materials has been shown to lead to a stiffening of the polymer due to the higher Young's Modulus of the filler.[3]

There are two additional ways in which the fillers can impact the mechanical properties of the polymer; (i) the interaction strength between the filler particles and the surrounding polymer matrix[4] and (ii) the degree to which the filler particles are dispersed within the polymer.[5] Based on this, researchers have employed several strategies to improve the mechanical properties of DEs. For example, Muriel et al.[4] modified the surface of SiO_2 particles, which enabled them to crosslink the particles with the copolymer resulting in a change of the composite structure. Also, they found the modified particles were better dispersed within the polymer matrix, which enhances the uniformity of the composite's elastic response.

Based on the geometry of fillers used in the polymer, there are two branches of filler material research. The first branch of research uses a spherical filler system. The mechanical

properties are improved by addition of a conducting material or metal oxide.[2] Both of them induce the stiffening effect and the value of stiffening is proportional to the concentration of the fillers. Suitable surface modification has been shown to improve the degree of covalent bonding and the compatibility of the filler with the polymer to avoid a debonding situation, which usually results in the existence of cracking mouths and laminate ends.[6,7,8]

The second branch of research uses asymmetric filler systems such as fibers, needles, or rod-like fillers.[9] The mechanical properties are mainly affected by the orientation of the fillers.[10] When the fillers are all aligned, the difference between the parallel and perpendicular direction are pronounced and the Young's Modulus parallel to the needles is larger than the Young's Modulus perpendicular to the needles. Compared to spherical fillers with similar surface areas and primary particles size, the fiber filled composite showed a larger toughness increase. [11]

So far, the use of an asymmetric, but spherical filler material, i.e., a Janus particle, has not been tested. In our study, Janus particles are produce by coating of spherical silica particles with a gold cap on one hemisphere. The change in bonding interaction and roughness difference causes the Janus particles to have different interaction strengths along their surface compared to unmodified silica filler materials and as a result impacts the composite structure. In this chapter, we will focus on elucidating the effect of Janus particle fillers on the mechanical properties of the p(EGPEA) elastomer.

5-2 Experimental Details for Elasticity Measurements

The elastic properties of the plain and composite p(EGPEA) films with 0.5% and 4% SiO_2 and 0.5% JP SiO_2 fillers are tested in tensile and compression mode using the texture analyzer and the nanoindenter, respectively.

5-2-1 Tensile Measurements

The stiffness of the pure, SiO_2, and JP SiO_2 p(EGPEA) thin films are measured using a texture analyzer (TA.HD.Plus/750, force resolution: 15g, force accuracy: 0.025%) equipped with a set of tensile test clamps. For tensile measurements, standard dog bone-shaped specimens[12] with a uniform thickness of 250 μm are made using a transparent PDMS mold, which is prepared with the help of an acrylic template, for the soft stamp replica molding technique.

Samples are strained at a speed of 2 mm/sec from an original working distance (initial distance between the two clamps) until a maximum force of 0.5 N is reached. The applied force is recorded as a function of specimen elongation. Three pieces of each type of film are measured at least three times in separate experimental runs. The force-distance data are collected in conjunction with the original cross-sectional area (250 μm x 2.5 mm) and length (1.70 cm).

5-2-2 Compression Measurements

An Asylum Research Nanoindenter is used for the analysis of elasticity and Young's Modulus in compression. The samples (surface area of 1"x1" with a thickness of 30 - 60 μm) are compressed at a constant speed of 5 μN/sec until the maximum force reached is within the range of 45 ~ 120 μN. The indentation depth is set such that it is 1 μm, which is less than 10% of film thickness and helps to avoid artificial effects from the hard surface on which the films are supported. The tip is held at the maximum force for another 20 seconds to reduce the effect of viscoelastic behavior of the elastomer on the measurement. In the end, the tip unloads the force at the same speed (5 μN/sec) by moving away from the sample surface.

Data points are collected when the compressive force is larger than the trigger force of 4.8 μN. The Young's Modulus is calculated in a range of 35 - 70 % of the applied force in the

return loop in conjunction with the stiffness (830 GPa) and Poisson's ratio (0.17) of the synthetic diamond tip. A glass slide is used as reference sample to determine the inherent accuracy of the nanoindentation measurement. The nanoindentation results collected for the glass slide forms a Gaussian distribution with a peak at ~80 GPa and a peak width of 27 GPa in good agreement with the values ranging from 50 to 90 GPa found in the literature.[13] Six samples of the plain and two composite films are measured. Each sample film is probed in more than 64 spots across the entire film surface (1" x 1").

5-2-3 Swelling Measurements

The swelling test requires a scale with an accuracy of 0.1 mg. The weight of the dried crosslinked polymer, W_p, is measured using the scale. Next, the polymer is immersed in an excess of solvent, e.g., toluene. After reaching the equilibrium of swelling (15 minutes), the polymer gel is removed from the solvent and the excess solvent on the surface of the polymer gel is dried using filter paper. Then, the weight of the solvent-swelled polymer (W_s + W_p) is determined. The swell ratio, ϕ_s, is calculated using the weight and density of both the polymer and toluene as shown in Equation 5-1.[14]

$$\phi_s = 1 + \frac{W_s/\rho_s}{W_p/\rho_p} \tag{5-1}$$

The second term in Eq. 5-1 is called the extract percentage of the swell ratio, ζ:

$$\zeta = \frac{W_s/\rho_s}{W_p/\rho_p} \tag{5-2}$$

5-2-4 UV/vis Measurements

To observe the effect of filler materials (silica and gold/titanium) on the photo-polymerization process, UV/vis spectroscopy (Thermo Scientific Evolution 300) is used to measure the UV light absorbance of silica and titanium/gold layers. The UV adsorption is measured for a transparent glass slide (thickness = 1.2 mm) and glass slides coated with 5/20, 5/30, and 5/40 nm of titanium/gold. The UV/vis absorption measurement is carried out using air as a background gas in the range from 300 to 500 nm.

5-2-5 TGA Measurements

In order to elucidate the effect of different fillers on the crosslinking degree obtained from photo-polymerization, we prepared pure films via three distinct curing processes; they are cured under a UV lamp (i) without cover, (ii) covered with a transparent glass slide (thickness: 1.2 mm), or (iii) a Ti/Au-coated glass slide (20 nm gold, 5 nm titanium and 1.2 mm glass slide). For these three types of pure films, we use ~10.5 mg of polymer in each measurement. The temperature range measured is from 50 ^{o}C to 550 ^{o}C with a heating rate of 10 ^{o}C/min. When the instrument reaches 600 ^{o}C, it is held isothermally for two minutes until the TGA curve stabilizes.

5-3 Results

In the following, the results from the tensile and compression measurements are presented.

5-3-1 Results from Tensile Measurements

Fig. 5-1 provides the stress-strain curves of three different type of films (pure p(EGPEA) – black lines, 0.5 vol% SiO_2-loaded p(PEGEA) – blue lines, and 0.5 vol% JP SiO_2-loaded p(PEGEA) – orange lines) obtained from tensile measurements of dog bone-shaped specimens

using the texture analyzer. Three samples for each type of composite are measured. As mentioned in Chapter 2, when the strain is small, we can assume that a dielectric polymer follows Hooke's law, i.e., the stress is proportional to the strain and the ratio of stress to strain in the elastic region of the stress-strain curve gives the Young's Modulus.

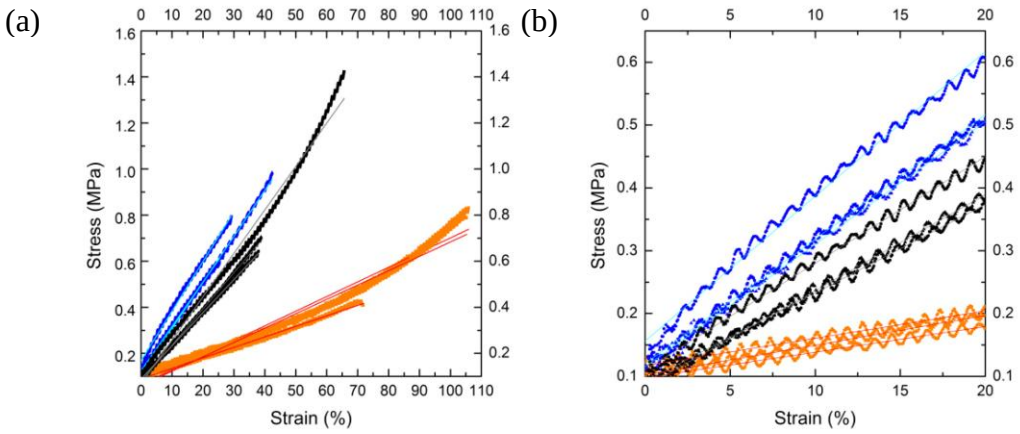

Fig. 5-1 Tensile measurement of dog bone-shaped samples. (A) Entire stress-strain response curve. (B) Zoomed-in region at origin of stress-strain curve. Black lines –pure p(EGPEA), blue lines -0.5 vol% SiO_2-loaded p(PEGEA), and orange lines - 0.5 vol% JP SiO_2-loaded p(PEGEA).

Table 5-1 lists the Young's Moduli determined from three sets of stress-strain curves depicted for each type of sample in Figure 5-1. Addition of unmodified SiO_2 particles leads to a slight stiffening of the polymer film ($Y_{SiO2\text{-}p(EGPEA)}$ = 2.08 ± 0.20 vs. $Y_{p(EGPEA)}$ = 1.54 ± 0.15). Surprisingly, the JP SiO_2-loaded p(EGPEA) composite films exhibit the lowest Young's Modulus ($Y_{JP\ SiO2\text{-}p(EGPEA)}$ = 0.44 ± 0.03 MPa) of all three films. Generally as discussed in Chapter 2-1-4, a stiffening of the polymer is expected upon addition of solid particles as seen in the case of the SiO_2-loaded p(EGPEA) films due to the hardness of the filler added. The possible reasons for the observed decrease of the Young's Modulus for the JP SiO_2-loaded p(EGPEA) films are discussed below.

The fluctuations observed in the zoomed-in data shown in Fig. 5-1 (b) are a representation of the limited resolution of the texture analyzer (see above). Factors that contribute to the noisiness of the data are the contact between clamp and film, the anisotropy of the material itself, and/or the non-uniformity of the applied tensile stress due to the stepping motor used for the force application. Because the resolution of the texture analyzer is limited compression experiments are done using nanoindentation.

TABLE 5-1 Young's Moduli of pure, SiO_2-loaded, and JP SiO_2-loaded p(EGPEA) polymer films determined form data shown in Figure 5-1.

Film	% load	Average [MPa]
Pure	0	1.54±0.15
SiO_2-loaded	0.5	2.08±0.20
JPSiO_2-loaded	0.5	0.44±0.03

5-3-2 Results from Compression Measurements

Fig. 5-2 provides histograms of Young's Moduli for the pure, SiO_2-loaded and JP SiO_2-loaded p(EGPEA) films obtained from compressive measurements using nanoindentation. Due to the point-by-point nature of the nanoindentation measurements, i.e., probing of a very small sample area many times, the Young's Moduli are analyzed using histograms to determine the most often measured modulus value. In Fig. 5-2 (a), the grey columns represent the distribution of nanoindentation result obtained for six pure p(EGPEA) elastomer films. Using a Gaussian curve fitting procedure, an elasticity of 3.76 MPa (peak maximum) is obtained for p(EGPEA) with a

probability distribution (peak width) of 0.87 MPa. The wide distribution of Young's Modulus values obtained is caused by the inherent uncertainty of the measurement technique, for example, small probe area, sample surface roughness, film stickiness, tip slipping on the surface and others. Fig. 5-2 (b) shows that the histogram for a 0.5 vol% SiO_2-loaded p(EGPEA) films (blue columns) can be fitted with a combination of two Gaussian distributions (black/blue lines) with the same peak width as obtained for the pure p(EGPEA) elastomer (0.87 MPa). The first (black) curve peaks at Y = 3.76 MPa, the same value measured for the pure p(EGPEA) elastomer, whereas the second, blue curve is situated at Y = 4.33 MPa (indicating a stiffer material). This part of the histogram is attributed to the presence of silica fillers within the elastomer. The increased hardness is in good agreement with the theory of filler reinforcement described in Chapter 2-1-4.

This observation is further supported by the results obtained for 4 vol% SiO_2-loaded p(EGPEA) films shown in Fig. 5-2 (c) as purple columns. Again, a combination of two Gaussian distributions with the same peak width (0.87 MPa) is used to determine the Young's Moduli. The first, black curve is located at Y = 3.76 MPa and represents the pure p(EGPEA) elastomer, while the purple line (4 vol% SiO_2) peaks at Y = 4.49 MPa, which is higher than the value obtained at a loading of 0.5 vol% SiO_2 in good agreement with the prediction from the theory of filler reinforcement (Chapter 2-1-4). The higher Young's Modulus is observed statistically more often in Figure 5-2 (c) because the higher filler concentration increases the probability of the nanoindentor to sense the existence of hard particles. A higher concentration of fillers will also lead to more filler-filler interactions and a stiffer material.

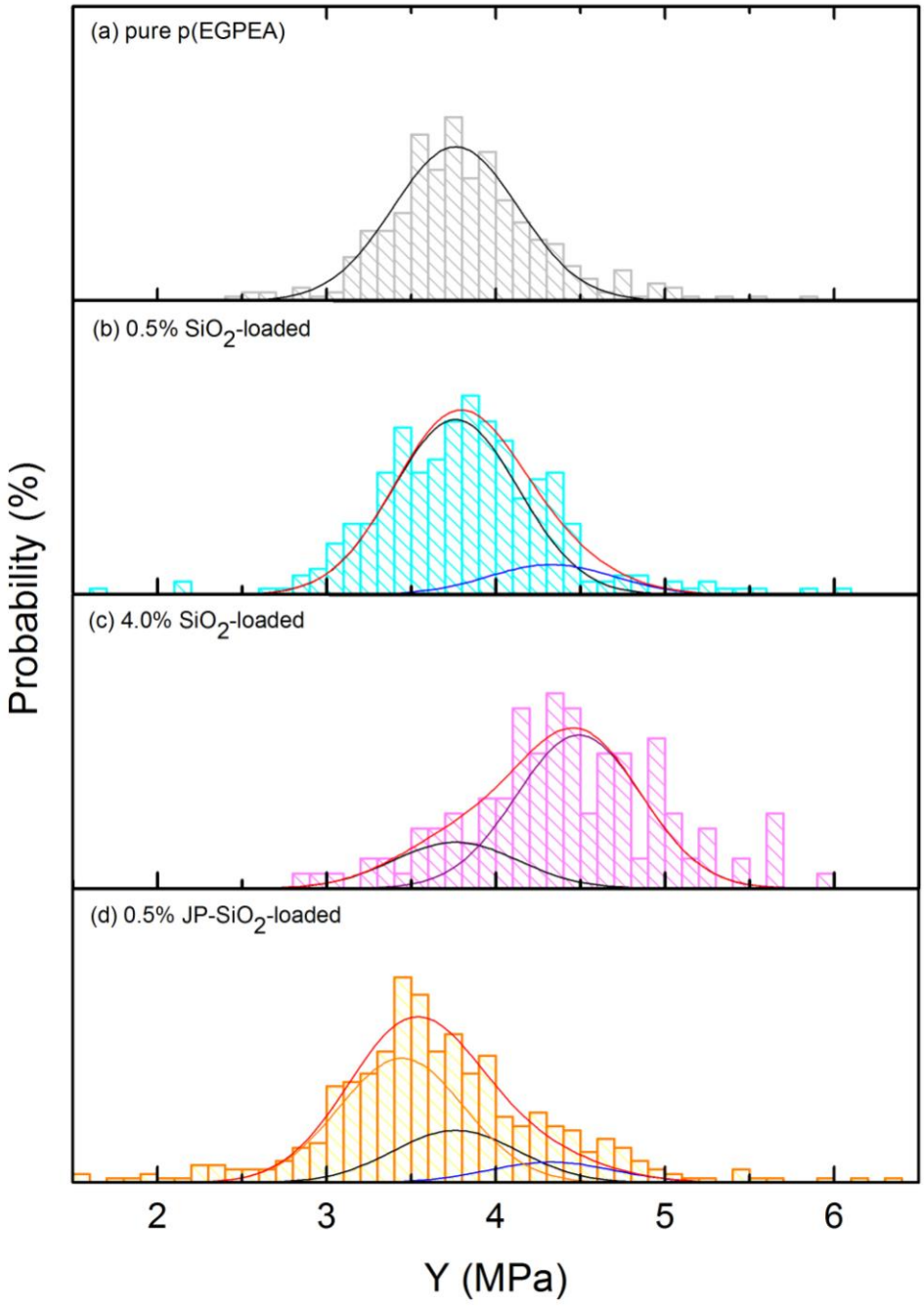

Fig. 5-2 Histograms for Young's Modulus measurements from nanoindentation experiments for (a) pure p(EGPEA) films, (b) 0.5 wt% SiO_2-loaded p(EGPEA) films, (c) 4 wt% SiO_2-loaded p(EGPEA) films, and (d) 0.5 wt% JP SiO_2-loaded p(EGPEA) films.

Note that $Y_{compression}$ is smaller than $Y_{tensile}$ due to the different specimen structure (thin film for compression and dog bone-shaped for tensile) resulting in the occurrence of the blocking force in the former. In addition, the Young's Moduli of pure films were also tested in compression using the texture analyzer (data not shown) confirming $Y_{compression,\ texture\ analyzer} > Y_{tensile,\ texture\ analyzer}$.

A fitting curve (red line) comprised of three curves is employed for the fit of the data shown in Fig. 5-2 (d) using a constant peak width of 0.87 MPa. The maxima of the three curves occur at Y = 3.44, 3.76, and 4.33 MPa, respectively. The curve with a maximum at Y = 4.33 MPa (blue line) is assigned to the contribution from the plain silica (a small percentage of particles does not get modified during JP fabrication), the curve peaking at Y = 3.76 MPa (black) is attributed to pure p(EGPEA), whereas the curve with the maximum at the lowest Young's Moduls (Y = 3.44 MPa) is assigned to the existence of JP SiO_2 fillers.

TABLE 5-2 Fitting Parameters obtained from fitting of Young's Modulus histograms shown in Fig. 5-2 obtained from nanoindentation compression tests of pure, SiO_2-loaded and JP SiO_2-loaded p(EGPEA) films.

Filler Material	Fitting Parameter	Orange	Black	Blue	Purple
Pure	Young's Modulus (Mpa)		3.76		
	Area (counts)		32.70		
	Peak Width (Mpa)		0.87		
0.5% SiO2	Young's Modulus (Mpa)		3.76	4.33	
	Area (counts)		25.30	4.35	
	Peak Width (Mpa)		0.87	0.87	
4.0% SiO2	Young's Modulus (Mpa)		3.76		4.49
	Area (counts)		2.85		9.48
	Peak Width (Mpa)		0.87		0.87
0.5% JP	Young's Modulus (Mpa)	3.44	3.76	4.33	
	Area (counts)	26.40	11.11	4.37	
	Peak Width (Mpa)	0.87	0.87	0.87	

The Young's Moduli obtained from fitting curves of the compressive measurement histograms are summarized in Table 5-2. The JP SiO_2 fillers show the lowest Young's Modulus peak at Y = 3.44 MPa. The SiO_2 fillers cause a stiffening of the polymer film compared to the pure p(EGPEA) films and this effect becomes more pronounced at higher silica particle loadings.

5-4 Discussion

In the following, the trends observed for the various fillers are compared to theoretical predictions. While the SiO_2 loaded films are found to agree well with the theoretical prediction, the JP SiO_2 loaded films deviate from the prediction. Potential reasons for this deviation are introduced and additional tests are performed to determine the cause for the observed trends.

5-4-1 Effect of Filler Materials on Young's Modulus

The effect of filler materials on the Young's Modulus of filler re-enforced composites has been studied by Guth and Simha (see Chapter 2).[3] Their equation (Eq. 2-15) can be used to predict the Young's Modulus increase based on the Young's Modulus of the pure polymer film and the vol% of filler added. Table 5-3 shows a comparison of the experimental weighted average Young's Modulus values with those predicted by Eq. 2-15.

TABLE 5-3 Young's Moduli of the various p(EGPEA) samples.

Sample	Weighted average	Guth & Simha's Theory Prediction	ΔY	Error
Pure	3.76±0.57			
0.5% SiO_2	3.85±0.59	3.81	0.04	1%
4.0% SiO_2	4.32±0.59	4.22	0.10	2%
0.5% JP SiO_2	3.62±0.67	3.81	-0.19	5%

According to Guth and Simha's Equation (Eq. 2-15), the addition of hard filler materials such as silica particles or JP SiO_2 particles to a polymer matrix should always enhance the overall Young's Modulus of the composite film. The experimental result for the 0.5 and 4 vol% SiO_2-loaded p(EGPEA) films are in good agreement with the predictions obtained from Eq. 2-15 demonstrating the accuracy of nanoindentation measurements. However, the decrease of the Young's Modulus for the JP SiO_2-loaded films does not agree with the Guth and Simha prediction. The only difference between the two filler materials is the presence of the 25 nm Ti/Au-cap in the case of the JP SiO_2 particles. There are three possible explanations for the observed softening of the JP SiO_2-loaded p(EGPEA) films; (i) the mixing process during the addition of particles causes the entrapment of air bubbles in the polymer, (ii) the gold prevents the curing of the polymer, and/or (iii) a component of the polymer precursor solution reacts with the gold section of the particle surface. Reason (i) air entrapment can be tested by swelling of the films in an organic solvent. Films containing air bubbles absorb more solvent than those without. Reason (ii) can be tested by use of UV/vis spectroscopy and TGA measurements, while verification of reason (iii) would require the use of attenuated total reflectance Fourier transform infrared spectroscopy (ATR-FTIR).[15]

5-4-2 Swelling of Polymer Films

Fig. 5-3 shows the extract percentage, ξ, obtained from swelling measurements for three different types of p(EGPEA) films for five independent specimens. The specimens are immersed in toluene solvent for 15 minutes to reach their toluene absorption equilibrium. There is very little difference in the ξ-values for the pure and composite films ($\xi_{p(EGPEA)}$ = 93 ± 7 % vs.

$\xi_{SiO2/p(EGPEA)}$ = 99 ± 4 %, and $\xi_{JP\text{-}iO2/p(EGPEA)}$ = 95 ± 7 %) confirming that air entrapment is not the cause for the observed change in the Young's Modulus.

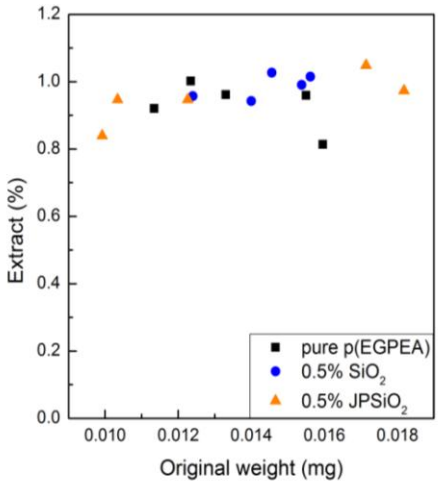

Fig. 5-3 Extract percentage, ξ, of three types of films; (a) pure p(EGPEA) films (black squares), (b) 0.5 wt% SiO_2-loaded p(EGPEA) films (blue circles), and (c) 0.5 wt% JP SiO_2- loaded p(EGPEA) films (orange triangles) obtained from swelling experiments.

5-4-3 Effect of Gold on UV/vis Transparency

Fig. 5-4 depicts the UV/vis absorption response of transparent glass and glass coated with titanium/gold layers of 5/20, 5/30, and 5/40 nm thickness in the range from 300 – 500 nm. The specific absorption values at a wavelength of 365 nm are 0.042, 0.959, 1.543 and 1.877, respectively. Using the transmittance-absorbance chart shown in Fig. 5-5, it is clear that only 10% of the 365 nm UV light is transmitted through a layer of 5/20 Ti/Au. In comparison, the plain glass slide allows 90% transmittance of 365 nm UV light. This observation points to the possibility that addition of JP SiO_2 fillers might interfere with the curing of the polymer matrix. This interference can leading to a reduction of Young's Modulus of the films due to blocking of the UV light near the gold face of the JP SiO_2 particles. Less UV light exposure would result in a

lower amount of crosslinking of the polymer leading to a more elastic behavior during tensile and compression tests.

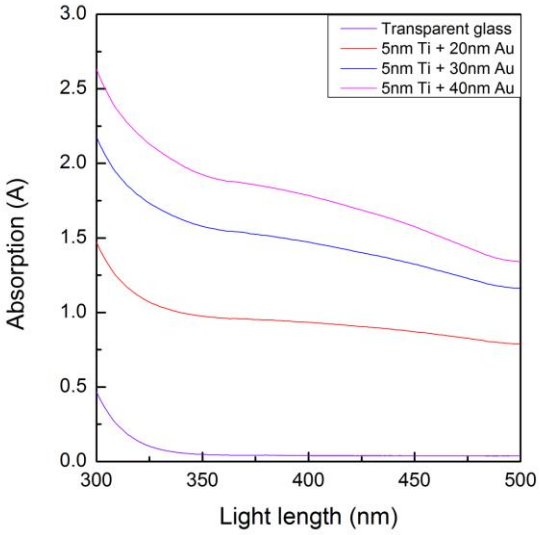

Fig. 5-4 UV/vis absorption measurements of plain glass slide (black line) and glass slides coated with 5/20 (red line), 5/30 (blue line), and 5/40 (magenta line) nm of titanium/gold.

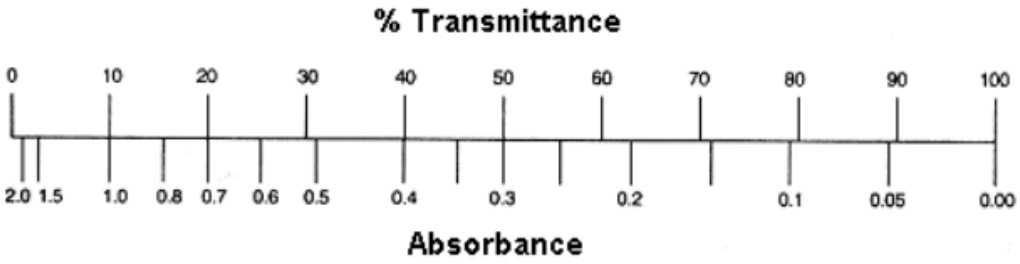

Fig. 5-5 Transmittance-absorbance conversion chart based on Beer's law.[16]

5-4-4 Thermogravimetric Analysis of Pure and Composite p(EGPEA) Films

In order to determine the effect of the reduced UV/vis transmission on the degree of crosslinking in the polymer, thermogravimetric analysis (TGA) is performed to measure the temperature/weight loss profiles for the pure film and pure films cured under a plain glass slide,

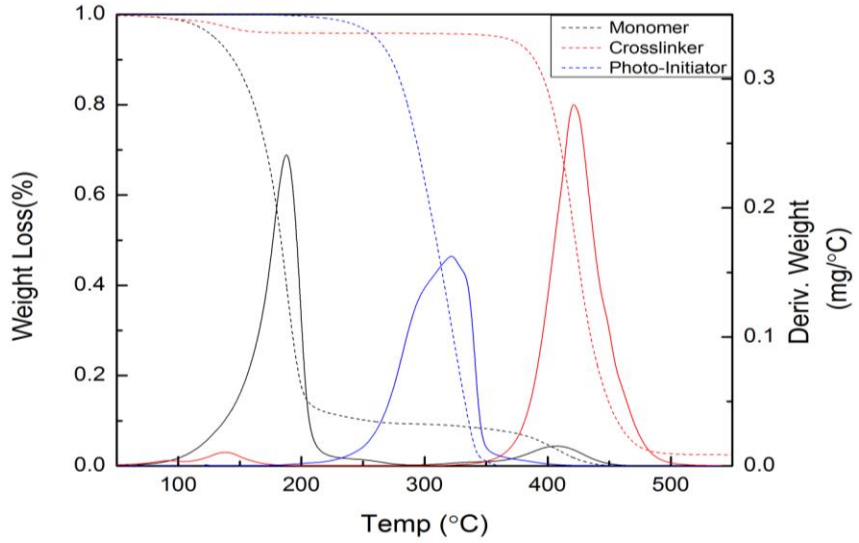

Fig. 5-6 Overlay of thermogravimetric analyses of the three pure components used in the precursor mixture. From left to right: ethylene glycol phenyl ether acrylate (black curve), 2-benzyl-2-(dimethylamino)-4'-morpholinobutyrophenone (blue curve), and 1,6-hexanediol diacrylate (red curve).

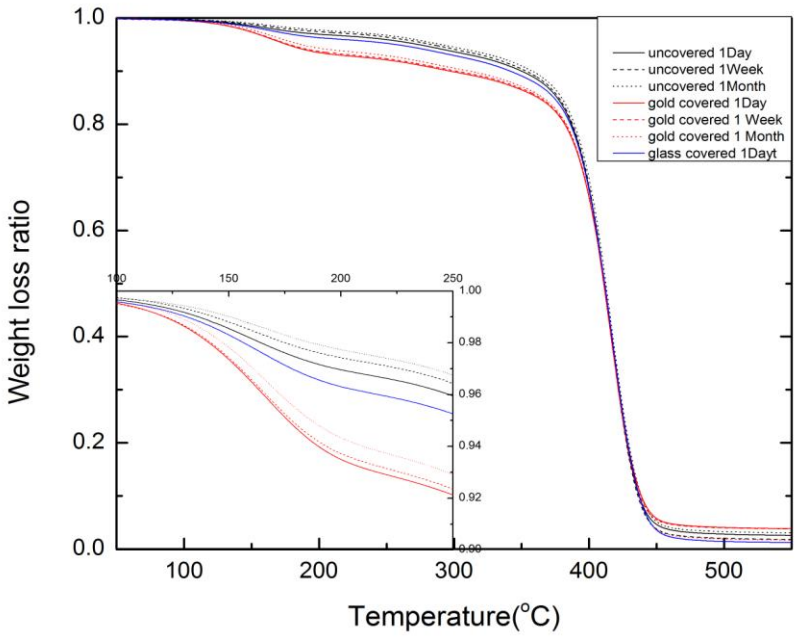

Fig. 5-7 Thermogravimetric analysis of pure p(EGPEA) films prepared via three distinct processing routes. From top to bottom: without obstruction (black lines), covered with a glass slide (blue line), and covered with a glass slide coated with a 5/20 Ti/Au layer (red lines). Solid, dashed and dotted lines indicate films measured 1 day, 1 week and 1 month post UV treatment.

and a glass slide with a 5/20 Ti/Au coating. In addition, the TGA spectra of the three components (photoinitiator/crosslinker/monomer) are measured in the range from 50 ^{o}C to 550 ^{o}C.

The thermal properties of the three pure components used in precursor mixture are determined individually by TGA from 50^{o}C to 550 ^{o}C. An overlay of their three TGA spectra is shown in Fig. 5-6. The monomer decomposes between 100 – 250 ^{o}C, the photoinitiator decomposes near 300 ^{o}C, and the crosslinker breaks down in the 400 – 450 ^{o}C range. Fig. 5-7 shows the TGA results for pure p(EGPEA) films cured under UV light without any obstruction (black lines), covered with a glass slide (blue line), and covered with a glass slide coated with a 5/20 Ti/Au layer (red lines). Each set of samples was measured 1 day (solid lines), 1 week (dashed lines), and 1 month (dotted lines) after curing to determine the post UV treatment behavior of the films. There are two apparent weight losses for all pure films shown in Fig. 5-7; the first loss is in the range from 100^{o}C - 250 ^{o}C (see inset for zoomed in version), the second one occurs between 380 ^{o}C - 460 ^{o}C. Further, we observed that the weight loss amount of the pure films decreases in Fig. 5-7 when measured one day vs. one month after curing, i.e., p(EGPEA) films self-cure as time passes. Comparison between Fig. 5-6 and Fig. 5-7 reveals that the first loss should be attributed to a loss of residual, non-crosslinked monomer within the polymer matrix, while the second one should be assigned to the loss of crosslinker. In addition, films covered with a Ti/Au coated glass slide exhibit more weight loss during the first weight drop compared to the films cured without any obstruction indicating that the gold layer causes the polymer film to have a lesser degree of crosslinking leaving uncured pre-polymer in the film.

In order to distinguish whether the reduction in crosslinking degree is due to the reduced UV exposure (reason ii) or to the reaction of the crosslinker (contains N-atoms with lone pairs)

with the gold cap (reason iii), nanoindentation measurements were obtained for three pure p(EGPEA) films cured without obstruction, with glass slide, and with Ti/Au coated glass slide after one day, one week, and one month post UV exposure. The films cured under the Ti/Au coated slide are found to be more elastic than those that were cured without any obstruction (Fig. 5-8, Table 5-4). Despite the fact that the films self-cure, the elastic properties of the films seem very consistent within one month (under gold-coated slide: 3.04, 2.99 and 3.00MPa vs. uncovered films: 3.36, 3.43, and 3.33 MPa). Therefore, we can conclude that the softening phenomenon observed for the JP SiO_2-loaded p(PEGEA) composite films is caused by the presence of the gold shells on the Janus Particles, which block the 365 nm UV light during polymerization resulting in less crosslinked polymer near the gold shells.

Note that the absolute Young's Modulus of pure p(EGPEA) without obstruction for the data shown in Fig. 5-8 is shifted to lower values compared to Figure 5-2 (3.36 vs. 3.76 MPa). This shift is a result of a less aged precursor mixture. Experiments with an aged precursor mixture show that the resulting polymer exhibits an increased Young's Modulus as the precursor mixture ages (data not shown). The rationale for this trend lies in the low vapor pressure of the monomer, which leads to evaporation of the monomer from the precursor mixture resulting in a higher crosslinker to monomer ratio and a more crosslinked, i.e., stiffer, polymer.

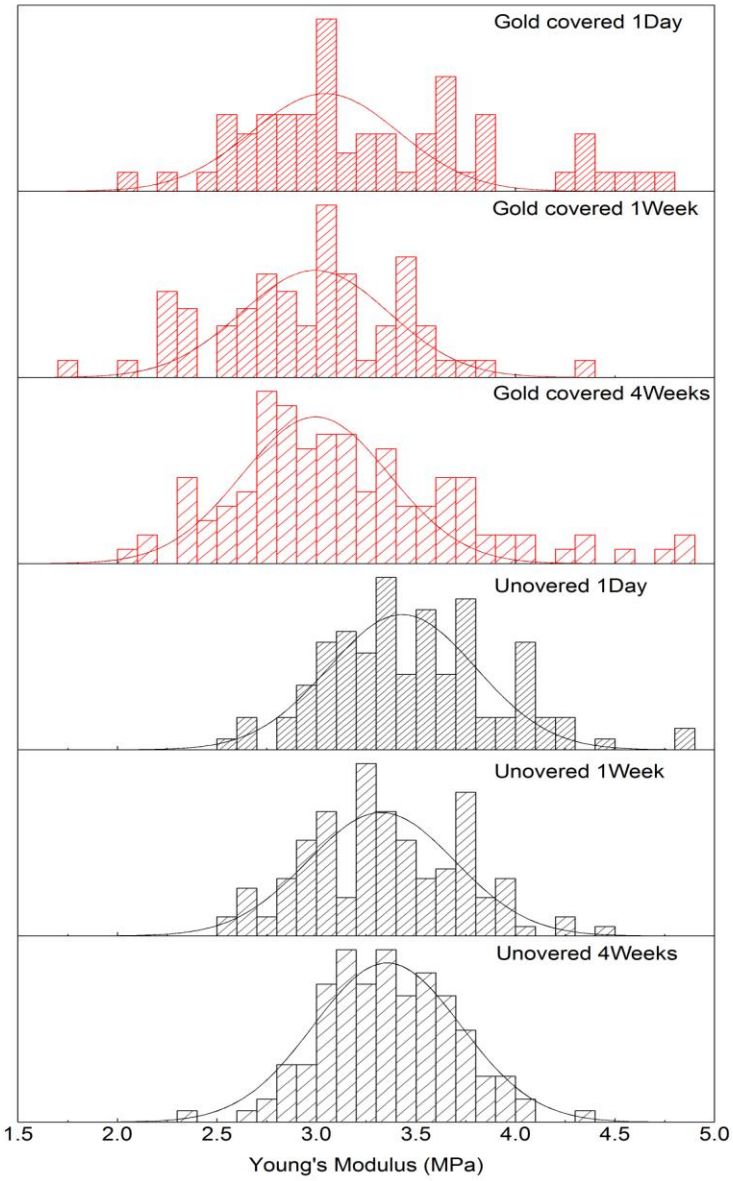

Fig. 5-8 Nanoindentation measurements for covered (top, red columns) and uncovered pure films (bottom, black columns) measured 1 day, 1 week, and 1 month post UV treatment.

TABLE 5-4 Fitting parameters obtained from fitting of Young's Modulus histograms shown in Fig. 5-8 obtained from nanoindentation compression tests of pure p(EGPEA) films cured under non-obstructed and obstructed UV/vis exposure.

Sample	Peak Center Position			σ^2
Gold covered 1 Day	Young's Modulus (Mpa)	**3.04**		0.53
	Area (counts)	4.74		
	Peak Width (Mpa)	0.87		
Gold covered 1 Week	Young's Modulus (Mpa)	**2.99**		0.64
	Area (counts)	5.77		
	Peak Width (Mpa)	0.87		
Gold covered 4 Weeks	Young's Modulus (Mpa)	**3.00**		0.76
	Area (counts)	9.48		
	Peak Width (Mpa)	0.87		
Uncovered 1 Day	Young's Modulus (Mpa)		**3.36**	0.96
	Area (counts)		12.87	
	Peak Width (Mpa)		0.87	
Uncovered 1 Week	Young's Modulus (Mpa)		**3.43**	0.80
	Area (counts)		11.65	
	Peak Width (Mpa)		0.87	
Uncovered 4 Weeks	Young's Modulus (Mpa)		**3.33**	0.78
	Area (counts)		11.96	
	Peak Width (Mpa)		0.87	

5-4 Summary

In this chapter, the mechanical properties of several pure and particle-loaded polymer films are presented and discussed in light of theoretical predictions. We find that films with silica particles are slightly stiffer ($Y_{tensile}$ = 1.54 ± 0.15 MPa and $Y_{compression}$ = 3.85 ± 0.59 MPa) than pure films ($Y_{tensile}$ = 2.08 ± 0.20 $Y_{compression}$ = 3.76 ± 0.57 MPa) in good agreement with the enforcement theory proposed by Guth and Simha. The addition of SiO_2 particle fillers causes an increase in the stiffness of the polymer. Further addition of more filler particles (i.e., 4 vol%)

results in even stiffer composite films. The weighted averages for the 0.5 and 4 vol% SiO_2-loaded films are 3.81 and 4.22 MPa and agree with Guth and Simha's prediction within 1-2 % error. In contrast, addition of JP SiO_2 particles leads to an unexpected reduction in Young's Modulus. Using UV/vis spectroscopy, TGA, and nanoindentation measurements, it is deduced that the presence of the gold cap is likely to cause a reduction in the amount of crosslinking due to the caps' lower UV transparency leading to a softer polymer film. The presence of air bubbles is excluded via swelling experiments. In order to rule out reaction of the components of the precursor mixture with the gold surface, reason (iii), further experiments are needed that involve ATR-FTIR.

Chapter Six – Dielectric Properties of Pure and Composite p(EGPEA) Films

6-1 Introduction

Electroactive polymers (EAPs) are able to deform in an external electric field. According to Maxwell's equation (Eq. 2-3) the compressive strain is proportional to the dielectric constant of the material itself. However, the dielectric constant of a dielectric elastomer is not as high as that of an ionic electroactive polymer. Hence, the addition of fillers with high dielectric constant is used as a general method to increase the overall dielectric constant of dielectric elastomers (DEs).

Researchers have added gold particles into a polymer matrix with the goal to enhance the overall dielectric constant of the material.[1] However, most metals have a negative dielectric constant at optical frequencies ($\nu = 10^{12}$ - 10^{15} Hz) according to the Drude Model.[2,3] Link et al.[4] state in their work that noble metals generally are able to increase the overall dielectric constant of a composite according to the Maxewell-Garnett theory.[5] In addition, the enhancement of the dielectric constant strongly depends on the aspect ratio of the added gold nanorods.[4] Here, we utilized the anisotropic structure of the Janus Particle with its very thin layer of gold on one side of the particle as carrier for the gold filler. Only 0.5 vol% of JP SiO_2 particles are added into the p(EGPEA) polymer matrix. To the best of our knowledge the dielectric properties of Janus particles in a polymer matrix have not been studied.

6-2 Experimental Details - Capacitance Measurements

Pure, 0.5 vol% SiO_2-loaded, and 0.5 vol% JP SiO_2-loaded p(EGPEA) films (d = 30-60 μm) placed on the conducting side of a square piece of FTO-glass (A_{FTO} = 1 in^2) are coated with

a circular 150 nm thick layer of aluminum (A_{Al} = 143-145 mm^2) by physical vapor deposition through a nickel hydroxide ($Ni(OH)_2$) mask at a deposition rate of 1 nm/s. Then, the film is placed on a probe station (Fig. 6-1 (a)) and the conducting side of the FTO glass slide and the aluminum layer are the two electrodes connected to the HP4284A LCR capacitance meter as shown in Fig. 6-1 (b).

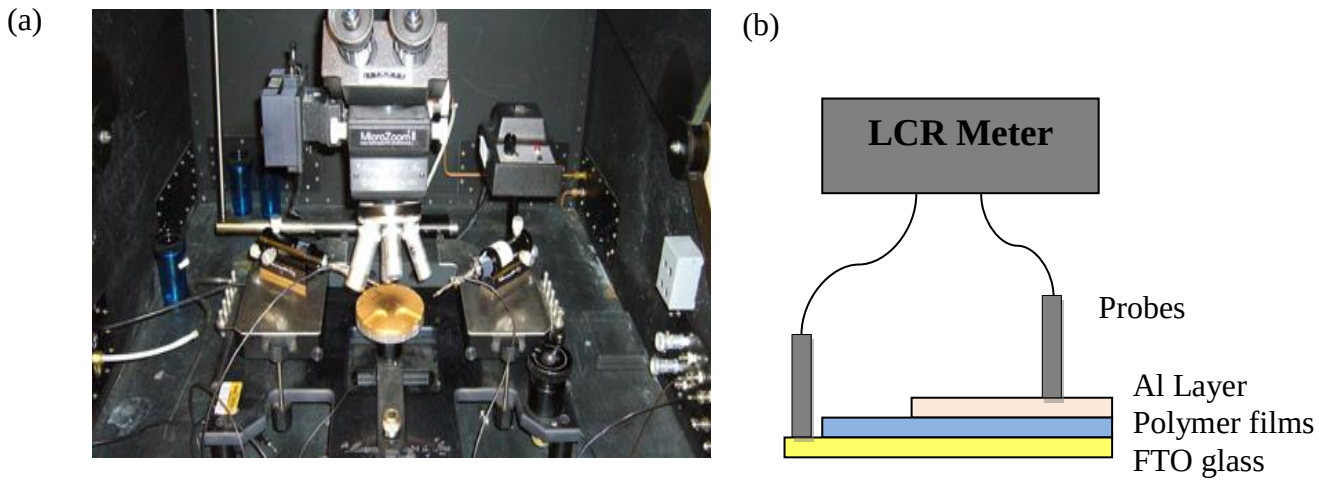

Fig. 6-1 Capacitance measurement set-up used for capacitance measurements.

Next, the capacitance and the dielectric loss are measured by the HP4284A LCR meter, which generates 0.5 V of an AC electric field with a frequency range from 100 Hz ~ 2 MHz. All measurements are done with four continuous loops within three minutes to avoid a dielectric loss increase due to heating of the films. Only data from the last three loops is used to allow for equilibration of the dielectric loss value.

The relative permittivity includes real and imaginary parts and both of them are dependent on the frequency of the electric field. At low frequencies, the relative permittivity is also called the static permittivity or relative dielectric constant, ε_r, which can be calculated from

the capacitance measurement in conjunction with the films thickness, the electrode cross sectional projected area, and the permittivity of vacuum, ε_o, for polymer film capacitors. Moreover, the dielectric loss (*tan* δ) can be read directly from the LCR meter and represents the ratio of imaginary part to real part, Equ. 6-5.

$$\varepsilon \rightarrow \hat{\varepsilon}(\omega) \tag{6-1}$$

$$\hat{\varepsilon}(\omega) = \varepsilon'(\omega) + i\varepsilon''(\omega) \tag{6-2}$$

$$\hat{\varepsilon}(\omega) = \varepsilon'(\omega) + i\frac{\sigma(\omega)}{\omega} \tag{6-3}$$

$$\varepsilon_r = \lim_{\omega \to 0} \hat{\varepsilon}(\omega) = \frac{t \times C_p}{A \times \varepsilon_o} \tag{6-4}$$

$$\tan\delta = \frac{\varepsilon''}{\varepsilon'} \tag{6-5}$$

6-3 Result

For calibration of the LCR meter and the capacitance set-up, a 50.8 μm thick Kapton film bought from DuPont is used as reference material. Its ε_r value is measured as 3.31 (see Fig. 6-2) in reasonable agreement with the literature value of 3.4 reported at a frequency of 1 kHz.[6]

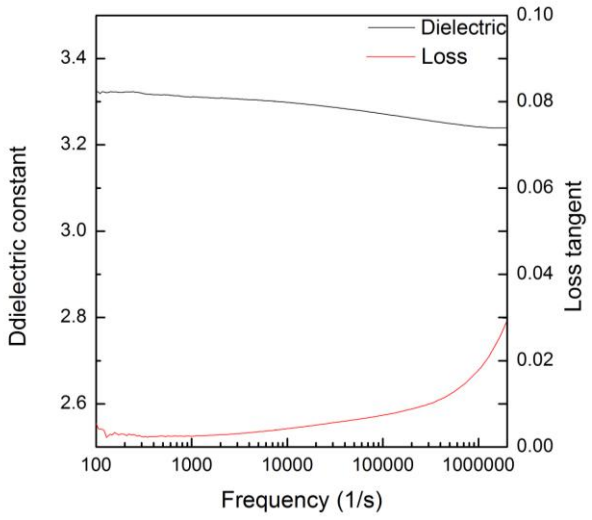

Fig. 6-2 Dielctric constant (left axis) and loss (right axis) for a Kapton film of 50.8 μm thickness.

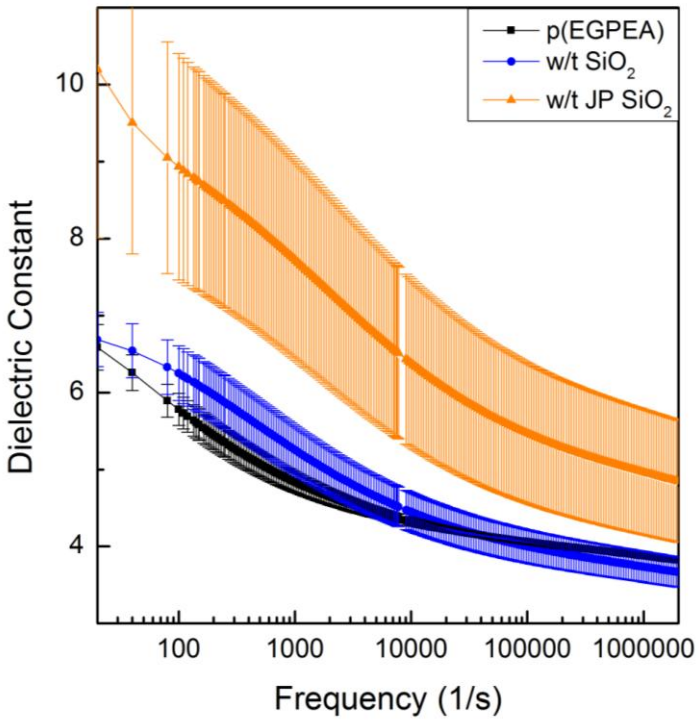

Fig. 6-3 Dielectric constant of p(EGPEA) films without filler (black line), with 0.5 vol% SiO_2 filler (blue line), and with 0.5 vol% JP SiO_2 fillers (orange line). The error range indicated is obtained by averaging the measurements from six independent films.

6-3-1 Relative Dielectric Constant (ε_r)

Fig. 6-3 depicts the dielectric constants measured for pure p(EGPEA) films (black line), 0.5 vol% SiO_2-loaded p(EGPEA) films (blue line), and 0.5 vol% JP SiO_2-loaded p(EGPEA) films (orange line) from six films prepared on different days. The dielectric constant measurements for the pure p(EGPEA) films are very reproducible and an ε_r value of 3.88 ± 0.04 is obtained at a frequency of 1 MHz. The dielectric constant measurement for the SiO_2-loaded p(EGPEA**)** composite shows more variation likely due to the non-ideal distribution of silica particles in the composites. The dielectric constant of SiO_2-loaded p(EGPEA**)** composite at 1 MHz is ε_r = 3.74 ± 0.20. Owing to the fact that the dielectric constants of bulk SiO_2 (ε_r = 3.9 @

1MHz[7]) and p(EGPEA) (ε_r = 3.88 ± 0.04) are very similar and only a very low concentration of SiO_2 filler is used, it is not surprising that their composite also has a similar dielectric constant as predicted by the mixing rule (Chapter 2-4-1).

However, in the lower frequency range (<30,000Hz), the dielectric constant of SiO_2-loaded p(EGPEA**)** composite increases to values higher than that of the pure p(EGPEA) film. This frequency range is dominated by molecular rearrangements (see Chapter 4-3), indicating that there is an interaction between the SiO_2 particles and p(EGPEA) elastomer that results in an increase of the composite's dielectric constant.

For example, a polymer with polar groups, such as C=O or OH groups, usually exhibits a high dipolar polarization resulting in a large dielectric constant at low frequencies. In addition, Morales-Acosta et al.[8] used FTIR experiments to prove the existence of OH bonds inside polymer composites loaded with SiO_2 particles and their effect on the dielectric constant. The increased dielectric constant at low frequencies in Fig. 6-3 may thus be attributed to the formation of OH bonds in the SiO_2-loaded p(EGPEA) films.

The JP SiO_2-loaded p(EGPEA) films exhibit the highest dielectric value with ε_r = 7.74 ± 1.30 (1 kHz) and 4.97 ± 0.82 (1 MHz). These values are much higher than any prediction by the Kerner theory (Eq.2-25) for a filler loading of 0.5 vol%. To understand the origin of this strong increase in dielectric constant, we return to curing the pure p(EGPEA) films without obstruction of the UV source and in the presence of a Ti/Au coated glass slide to simulate the effect of the gold cap on the dielectric constant of the cured films.

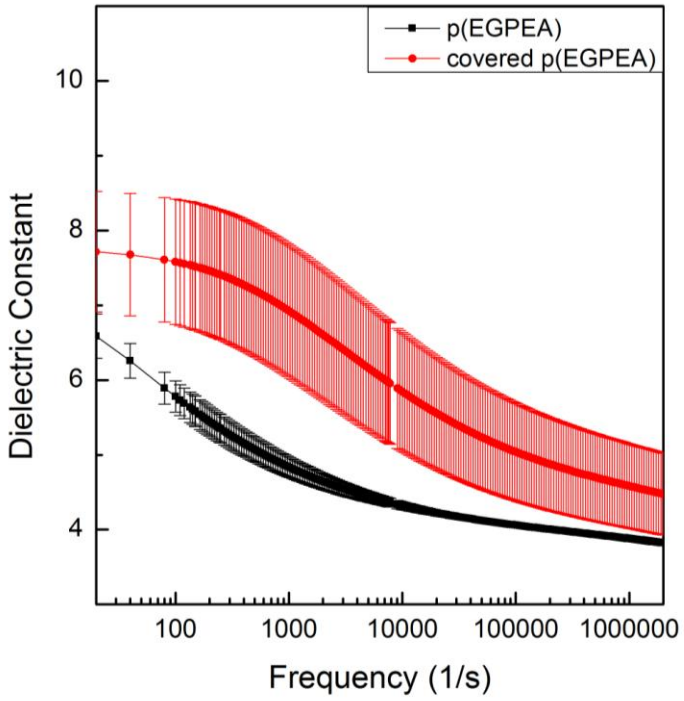

Fig. 6-4 Dielectric constant measurements for pure p(EGPEA) films cured under unobstructed UV light (black line) and under a glass slide coated with a 5/20 Ti/Au layer (red line).

6-3-2 Dielectric Constant of Pure Films Cured Under Obstructed and Unobstructed UV Conditions

Fig. 6-4 shows the dielectric constant measurements for pure p(EGPEA) films cured under unobstructed UV light (black lines) and cured in the presence of a glass slide coated with a 5/20 nm layer of Ti/Au (red lines). The dielectric constants of pure p(EGPEA) films cured in the presence of the gold layer are much higher than those of pure p(EGPEA) films cured without any obstruction.

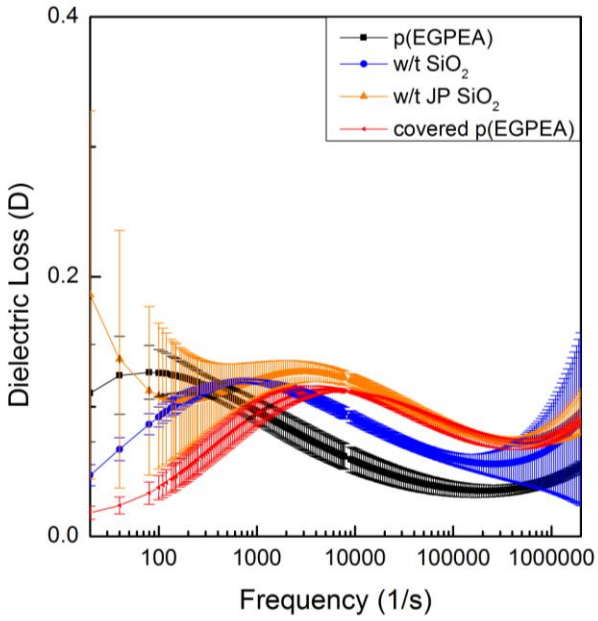

Fig. 6-5 Loss tangent of pure (black line), SiO_2-loaded (blue line), JP SiO_2-loaded p(EGPEA) films (orange line) and pure p(EGPEA) films cured under a glass slide with a 5/20 Ti/Au coating (red line).

6-3-3 Dielectric Loss Tangent (*tan*δ)

For an electro-mechanical actuator, the energy efficiency is strongly related to the dielectric loss of the material. Fig. 6-5 provides the $\log_{10}$ relationship between dielectric loss and frequency. In Fig. 6-5, all dielectric loss tangent values of films are below 0.2, which is very low. A film with a low dielectric loss represents (i) a film with good electrical performance, (ii) the possibility of longer term use, and (ii) higher energy transfer efficiency. The high energy efficiency indicates that the film has a very good fabrication structure for use as a capacitor.

The error range for the JP SiO_2-loaded p(EGPEA) film is much high than that of the other three films tested in the low frequency range (< 1,000 Hz). The unstable dielectric loss at low frequencies indicates high sensitivity to temperature and humidity. The SiO_2-loaded p(EGPEA) film has a large error at higher frequencies (> 100,000 Hz). An increase of the dielectric loss at

higher frequency indicates an inappropriate capacitor structure, such as a bad contact between electrodes and power supply. Furthermore, the loss values for all four films increase at frequencies above 1 MHz. This increase observed at high frequencies can be attributed to the imperfect AC circuit used in the measurement. Dielectric loss measurements are most reliable in the 1 kHz to 1 MHz frequency range.

The dielectric loss of pure p(EGPEA) films is 0.097 ± 0.009 and 0.043±0.004 at 1 kHz and 1 MHz, respectively, and represents the lowest dielectric loss of all four film types measured. The higher overall dielectric loss for composite films loaded with SiO_2 (0.119±0.001 and 0.068±0.034 at 1 kHz and 1 MHz, respectively) is expected due to the interface between fillers and the polymer matrix. The JP SiO_2-loaded p(EGPEA) composite films exhibit the highest dielectric loss of 0.120 ± 0.014 and 0.079 ± 0.008 at 1 kHz and 1 MHz, respectively, indicating that Janus particles are good candidates as fillers because they only cause a very small additional energy loss but strongly enhance the overall dielectric constant of the composite. The pure p(EGPEA) film cured under obstructed UV light shows a dielectric loss that is very similar to that of the JP SiO_2-loaded p(EGPEA) film. Interestingly, the noise in the loss at low frequencies is much less pronounced for these films indicating that the response in this range for the JP SiO_2-loaded p(EGPEA) film is dominated by the presence of the Ti/Au capped Janus particles.

6-4 Discussion

Table 6-1 lists the dielectric constants of various filler loaded p(EGPEA) films measured at 1 kHz and 1 MHz and compares them with the dielectric constant of pure p(EGPEA) films. The dielectric constant of 0.5 vol% SiO_2-loaded p(EGPEA) films is very similar to pure

p(EGPEA) films due to the similarity of the dielectric constant between SiO_2 particles and p(EGPEA) elastomer. However, the dielectric constant of JP SiO_2-loaded films shows a pronounced enhancement compared to both pure p(EGPEA) films and 0.5 vol% SiO_2-loaded composite films. Potential reasons for this enhancement may be (i) a higher dielectric constant of the p(EGPEA) polymer due to the reduced transmission of UV light in the gold cap regions, (ii) higher dielectric constant of gold caps, and/or (iii) the anisotropic nature of the Janus particles.

Calculating the maximum possible projected area of gold shells in a 0.5 vol% JP SiO_2-loaded p(EGPEA) film gives an area of 3.7 mm^2, which is much smaller (0.3 %) than the total polymer area on FTO glass slide (645 mm^2). This implies that the maximum contribution due to UV transmission reduction form the coverage of the gold caps is 0.3 % much less than the enhancement observed in Figure 6-3. Therefore, we conclude that the majority of the enhancement of the dielectric constant in the JP SiO_2-loaded films results from the anisotropy of the Janus particles in combination with the contribution of the gold caps to the dielectric constant of the composite.

An additional advantage of the JP SiO_2 fillers is that only part of their surface is coated with gold instead of their entire surface, i.e., core-shell particle. Gold particles have a strong tendency to aggregate and the Janus particle structure reduces this aggregation propensity allowing for better dispersion.

TABLE 6-1 Dielectric constant of films with different fillers.

	ε_r @ 1k Hz	ε_r @ 1M Hz
p(EGPEA)	4.84±0.14	3.88±0.04
w/t SiO_2	5.27±0.32	3.74±0.20
w/t SiO_2 JP	7.74±1.30	4.97±0.82
Covered p(EGPEA)	6.94±0.89	4.58±0.57

TABLE 6-2 Loss tangent of films with different fillers.

	D @ 1k Hz	D @ 1M Hz
p(EGPEA)	0.097±0.009	0.043±0.004
w/t SiO_2	0.119±0.001	0.068±0.034
w/t SiO_2 JP	0.120±0.014	0.079±0.008
Covered p(EGPEA)	0.094±0.009	0.075±0.003

6-5 Summary

In this chapter, evidence is provided that the addition of JP SiO_2 particles results in a higher dielectric constant for the 0.5 vol% JP SiO_2-loaded p(EGPEA) composite films compared to both pure p(EGPEA) films and SiO_2-loaded p(EGPEA) composite films. It is also shown that the increase in the dielectric constant is not only caused by the reduced curing in the areas near the caps, but that most of the enhancement must be a result of the anisotropic nature of the Janus particles and/or the dielectric constant contribution of the gold caps. In the future, the overall dielectric constant of the JP SiO_2 filler needs to be calculated employing the three components of the Kerner model to support the experimental results.

Chapter Seven – Electro-Mechanical Actuation of Pure and Loaded p(EGPEA) Films

7-1 Introduction

Dielectric electroactive polymers (EAPs) are polymeric materials that respond with a mechanical strain when they are exposed to an electric field. In response to the electrode's electrostatic attraction, the dielectric polymer films are able to compress by reducing their thickness along the direction of the electric field and by elongating in the transverse direction. The electromechanical mechanism (also known as Maxwell Strain Response)[1] of dielectric EAPs can be described by Eq. 2-3, where $|S_z|$ is the absolute value of the strain response, ε_o is the dielectric constant of vacuum, ε_r is the relative dielectric constant of the material, Y is the Young's Modulus, and E is the electric field. Dielectric EAPs can be employed in actuator applications such as the motor of automobiles, robots, fluidic pumps and hydraulic pistons, loud speakers, switches, and responsive haptic displays due to properties such as high elasticity, rapid response, and low power consumption.[2]

However, dielectric EAPs usually have the problem that their high dielectric constant is directly coupled to their mechanical properties, i.e., a material with a higher dielectric constant usually exhibits also a high Young's modulus. A material with a high Young's Modulus is mechanically stiff and requires a high actuation voltage (150 V/μm).[2] If the dielectric constant could be decoupled from the Young's Modulus of the dielectric elastomers, it might be feasible to create dielectric elastomer films that can be actuated at much lower operating voltages, i.e., 13 V/μm.[3]

In this chapter, we report results on the electroactive behavior of Janus particle-filled polyethylene glycol phenyl ether acrylate, JP SiO_2-loaded p(EGPEA), films. We have shown that addition of Janus particles decreases the films Young's Modulus (Chapter 5) and increases the dielectric constant of the p(EGPEA) material (Chapter 6). Testing of the electrostrictive polymer films under voltage load shows an enhanced response of JP SiO_2-filled p(EGPEA) films compared to pure and SiO_2-filled p(EGPEA) films.

7-2 Experimental Details – Actuation Response Measurements

An optical surface profiler (Wyko NT1100) with a 20x objective and 1.0x field of view is used to measure the actuation deformation of the thin films on the FTO glass plate. This measurement technique provides a non-contact method that enables us to measure changes in thickness of the pure, SiO_2-loaded, and JP SiO_2-loaded p(EGPEA) thin films, while avoiding harm to their flexible surface. For the WYKO NT1100, a tungsten halogen lamp projects filtered light from a white-light source (centered at 632 nm) to generate interference fringes. After the interferometry set-up has captured the fringe, Wyko vision® software is used to analyze the optical signal and convert it into data that allows the reconstruction of 2D or 3D maps of the measured surface. Figure 7-1 shows a schematic of the experimental setup. A 5-by-2 mm^2 plate made from a Si-wafer coated with gold (yellow) is placed on top of the film (blue). The plate is connected to the positive electrode of the DC power supply (Keithley 248, high voltage supply) by a fine, flexible gold wire (D = 0.001"), which is connected to a thicker copper wire further away from the structure. A voltage in the range from 50 to 450 V is applied between the plate on top of the films and the conducting side of the FTO plate, which is in contact with the bottom of

the film. the maximum applied voltage is kept well below the breakdown voltage of the pure film (~700V) and the composites (550V).The electric field is increased in 1 V/μm steps during measurement and height changes are recorded leading to stress/strain curves. The films for these measurements are prepared as described in Chapter 3-3.

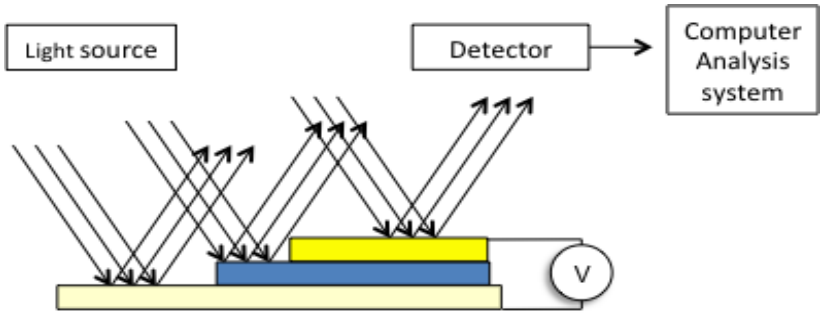

Fig. 7-1 Measurement set-up for electroactivity measurements.

7-3 Result

All films show compressive behavior upon application of an electric field. The compressive strain responses of one pure, one SiO_2, and four JP SiO_2-loaded p(EGPEA) films are shown in Figure 7-2. The black squares represent the response of a pure p(EGPEA) film, the red circles display the response of a SiO_2-loaded p(EGPEA) composite film, and the triangles of various colors and orientation represent responses from the four JP SiO_2-loaded p(EGPEA) composite films. Error bars are the result of three measurements per film.

According to Eq. 2-3 that describes the Maxwell Strain, which relates the observed strain to the electrostatic force applied by the external field, the slopes of the lines in Figure 7-2 are a representation of the experimental electrostrictive coefficient (S_{exp}). The S_{exp} values measured for

the one pure, one SiO_2-loaded, and four JP SiO_2-loaded p(EGPEA) composite films are summarized in the last column of Table 7-1. The response from the JP SiO_2-loaded p(EGPEA) films resulting in S_{exp} values ranging from 7.01 to 54.59 × 10^{-16} m^2/V^2 is clearly higher than the S_{exp} values of 0.69 and 2.36 × 10^{-16} m^2/V^2 measured for the pure and SiO_2-loaded p(EGPEA) films, respectively.

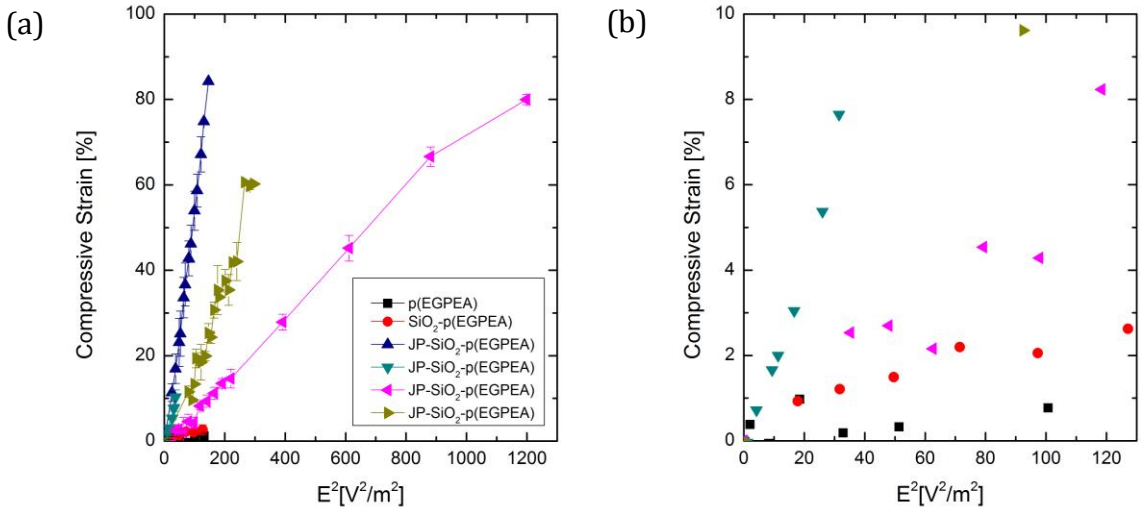

Fig. 7-2 (a) Entire compressive strain response and (b) zoomed-in region of compressive strain response as a function of the square of the electric field for a pure (black squares), a SiO_2-filled (red circle), and four JP SiO_2-filled p(EGPEA) films (various colors, triangles). Thicknesses for the JP SiO_2-filled p(EGPEA) films are 10 μm (up triangles), 47 μm (down triangles), 5 μm (triangles pointing right), and 10 μm (triangles pointing left).

Eq. 2-3 also shows that the theoretical electrostrictive coefficient (S_{theo}) is proportional to the overall dielectric constant ($\varepsilon_o\varepsilon_r$) and inversely proportional to the Young's Modulus (Y) of the polymer films. S_{theo} describes the ability of polymer films to deform due to electrostatic

interactions between small domains inside the p(EGPEA). The relative dielectric constants and the Young's Modulus values of pure, SiO_2-loaded, and JP SiO_2-loaded p(EGPEA) films derived from the tensile measurements (Chapter 5) and capacitance measurement (Chapter 6) are listed in Table 7-1. The dielectric constant values obtained at 20 Hz are used here since a low frequency AC field is similar to a DC field. The capacitance measurements confirm that Janus particles increase the overall dielectric constant of the composite, which may be attribute to their heterogeneous nature and ability to carry a high local dipole moment in an electric field and/or the higher dielectric constant of gold caps as shown by the increased relative dielectric constant of the JP SiO_2-loaded p(EGPEA) composite (ε_r = 10.20 ± 2.19 at 20Hz) compared to the pure (ε_r = 6.59 ± 0.30 at 20 Hz) and SiO_2-loaded p(EGPEA) films (ε_r = 6.69 ± 0.35 at 20 Hz). The weighted average Young's Modulus values derived from the nanoindentation compression tests (Chapter 5) are given in the second column of Table 7-1. Interestingly, the JP SiO_2-loaded p(EGPEA) films exhibit the lowest Young's Modulus ($Y_{JP(SiO2)\text{-}p(EGPEA)}$ = 3.62 ± 0.67 MPa) of all three films. Generally, a stiffening of polymers is expected upon addition of solid particles as seen in the case of the SiO_2-p(EGPEA) films. However, as shown in Chapter 5, the presence of the gold shell leads to partial blocking of the 365 nm UV light resulting in a more elastic p(EGPEA) polymer. Addition of unmodified SiO_2 particles leads to a slight stiffening of the polymer film ($Y_{SiO2\text{-}p(EGPEA)}$ = 3.85 ± 0.59 vs. $Y_{p(EGPEA)}$ = 3.76 ± 0.57). Combination of the two effects (ε_r and Y) results in a higher theoretical electrostrictive coefficient (S_{theo}) predicted by Eq. 2-3, for the JP SiO_2-loaded p(EGPEA) film in good agreement with the tendency observed from the actuation measurements shown in Fig. 7-2.

TABLE 7-1. Young's Modulus (*Y*), relative dielectric constant (ε_r), theoretically predicted (S_{theo}) and experimentally measured electrostrictive coefficient (S_{exp}) for pure, SiO_2-loaded and JP SiO_2-loaded p(EGPEA) films.

Type of Film	ε_r@20Hz [no unit]	Weighted average Y [MPa]	S_{theo} [10^{-16} m^2/V^2]	S_{exp} [10^{-16} m^2/V^2]
p(EGPEA)	6.59	3.76±0.57	0.155	0.69
SiO_2-p(EGPEA)	6.69	3.85±0.59	0.154	2.36
JP SiO_2-p(EGPEA)	10.20	3.62±0.67	0.249	7.01/18.92/23.88/54.59

The use of electrostriction (S) as a figure of merit when determining the strain-stress responses is appropriate for the work reported here, but cannot be generalized for use in the area of device fabrication. For example, materials with high S values have a higher energy density, but their Young's Modulus may be too low and thereby limit the practical use as an actuator as their low tensile strength does not provide enough "push-back" force (see Chapter 4-2-1).

7-4 Discussion

In most dielectric EAPs, the electrostrictive coefficient, *S*, is less than 1×10^{-18} m^2/V^2 resulting in an electrostrictive strain of 0.01 in a field of 100 $V/\mu m$[4]. However, more recently, electrostrictive coefficients as high as 10×10^{-16} m^2/V^2 have been reported.[5-7] An overall enhancement of the performance of p(EGPEA) as a result of Janus particle filler addition is observed in the external E-field induced strain measurements. The maximum compressive strain

measured is as high as 85% indicating an electrostrictive coefficient as high as 55×10^{-16} m^2/V^2 (Table 7-1). The overall increase of the relative dielectric constant and the decrease of the Young's Modulus confirm the higher electrostrictive coefficient for the JP SiO_2-loaded p(EGPEA) composite films in good agreement with the trends observed in the experimental S_{exp} values. However, the theoretically predicted electrostrictive coefficient, S_{theo}, is an order of magnitude smaller than the experimental value, S_{exp}. A possible reason for the much higher experimental electrostrictive coefficient is that the strain response mechanism may not be solely caused by the Maxwell Effect but also by an electrostrictive behavior of the polymer, which is not captured by Eq 2-3. On the other hand, an entirely different actuation mechanism involving electrets[8] may be accessed in JP SiO_2-loaded polymers, due to the macro dipole of the Janus particles, which may cause Janus particles to be partially aligned when the initial electric field is applied. In future work, we will further investigate the electro-mechanic mechanism of the JP SiO_2-loaded p(EGPEA) films. In addition, as can be seen from Figure 7-2, the response of the films, while uniform within one film, is not yet uniform across different films and additional experiments are required to investigate the origin of the variation. Potential reasons for the variation are uniformity of particle distribution and a random orientation of the Janus particles within the film.

7-5 Summary

Pure p(EGPEA) and SiO_2- and JP SiO_2-filled p(EGPEA) films loaded with 0.5 vol% of 500 nm SiO_2- and JP SiO_2 particles, respectively, have been prepared by a transparent PDMS soft-stamp method. JP SiO_2-filled p(EGPEA) films are found to show high compressive response

at low electric fields (85% at 12 V/m) due to an increased electrostictive coefficient (S_{exp} = 54.59 × 10^{-16} m^2/V^2). Characterization of the films' relative dielectric constant and Young's Modulus leads to the prediction of a theoretical electrostrictive coefficient (S_{theo} = 0.25 × 10^{-16} m^2/V^2) that is also higher than that of the pure and SiO_2-loaded p(EGPEA) films. However, the S_{theo} value is an order of magnitude lower than the S_{exp} value pointing towards the presence of actuation mechanisms other than the Maxwell Effect such as electret actuation. In addition, while the film response is clearly reproducible, large film-to-film variation is observed and further investigation of the effect of Janus particle orientation and dispersion is needed.

Chapter Eight – Summary and Future Works

8-1 Summary

The increasing energy demand has pushed researchers to explore new avenues of energy harvesting involving natural forces such as wind and ocean waves. Further, the need for devices that can provide tactile feedback has created a need for cheap materials that can replace piezoelectric materials. Both applications have in common that they require the interconversion of mechanical and electrical energy and *vice versa*. Dielectric elastomers stand out as one class of electroactive polymers that can be employed as actuators owing to their low cost, weight, and power consumption in combination with fast response and high flexibility, which make them suited for application as actuators. However, they are often limited in their applicability due to the proportional relationship between their Young's Modulus and their dielectric constant, e.g., a high dielectric constant usually combines with a high Young's Modulus requiring a large actuation field. Addition of high dielectric fillers to dielectric elastomers has been shown to enhance the overall dielectric constant of the composite, while only slightly affecting the flexibility of the elastomers.

In this thesis, the actuation behavior of one particular kind of dielectric elastomer, i.e., poly ethylene glycol phenyl ether acrylate, p(EGPEA), has been studied. The effect of 500 nm plain silica (SiO_2) and titanium/gold (5/20nm) capped SiO_2 Janus particles (JP SiO_2) on the Young's Modulus, the dielectric constant, and the actuation behavior has been tested. p(EGPEA) films are prepared from a precursor 96:3:1 mixture of EGPEA monomer, 1,6-hexanediol

diacrylate (cross linker), and photoinitiater using a PDMS soft molding technique. 500 nm JP SiO_2 filler particles were fabricated by a combination of convective assembly and thermal evaporation of 5 nm Ti and 20 nm Au. The resulting pure, SiO_2-loaded and JP SiO_2-loaded p(EGPEA) films are characterized using texture analyzer and nanoindentation testing (Young's Modulus), capacitance measurements (dielectric constant and loss), and optical profiling (actuation).

As presented in Chapter 5, the Young's Modulus of pure p(EGPEA) films is determined as $Y_{tensile}$ = 1.54 ± 0.15 MPa and $Y_{compression}$ = 3.76 ± 0.57 MPa from texture analyzer and nanoindentation testing, respectively. Addition of 500 nm SiO_2 particles into the p(EGPEA) matrix at 0.5 and 4 vol% increases the film stiffness to $Y_{SiO2\text{-}p(EGPEA),\ tensile}$ = 2.08 ± 0.20/$Y_{SiO2\text{-}p(EGPEA),\ compression}$ = 3.85 ± 0.59 MPa and $Y_{SiO2\text{-}p(EGPEA),\ compression}$ = 4.32 ± 0.59 MPa, respectively. This increase is in excellent agreement (deviation < 1-2 %) with the enforcement theory proposed by Guth and Simha.[1] In contrast, addition of JP SiO_2 filler particles leads to an unexpected reduction in the Young's modulus of $Y_{JP\ SiO2\text{-}p(EGPEA),\ tensile}$ = 0.44 ± 0.03 MPa and $Y_{JP\ SiO2\text{-}p(EGPEA),\ compression}$ = 3.62 ± 0.67 MPa. Since the same trend is observed both in the tensile and the compression measurements, experimental and instrumentation errors were excluded as possible reasons for this decrease. Swelling tests are used to exclude the entrapment of air bubbles during the mixing as a possible origin of the lower Young's Modulus. UV/vis spectroscopy reveals that the 5/20nm Ti/Au layer blocks 90% of the UV radiation at 365 nm reducing the amount of crosslinking during the UV treatment. Thermogravimetric analysis confirms that the presence of the Ti/Au layer causes a larger amount of unreacted EGPEA

monomers in the films leading to a softening of the films. Further analysis is needed as to what the exact local microstructure around the Janus particles is inside the polymer.

In Chapter 6 the dielectric constants of pure, SiO_2-loaded, and JP SiO_2-loaded p(EGPEA) films have been presented. Good agreement with literature values is found for the pure p(EGPEA) polymer ($\varepsilon_{r,p(EGPEA)}$ = 4.84 ± 0.14 and 3.88 ± 0.04 at 1kHz and 1MHz, respectively). Dielectric constants for the SiO_2-loaded p(EGPEA) films are measured as $\varepsilon_{r,sio2/p(EGPEA)}$ = 5.27 ± 0.32 and 3.74 ± 0.20 at 1 kHz and 1 MHz, respectively. The dielectric constant of pure and SiO_2-loaded p(EGPEA) films are very similar at 1 MHz in good agreement with the similar dielectric constants of SiO_2 (3.90 at 1 MHz) and p(EGPEA) (3.88 at 1 MHz). The addition of 0.5 vol% of JP SiO_2 filler particles results in an increase of the dielectric constant of JP SiO_2-loaded p(EGPEA) films, i.e., ε_r = 7.74 ± 1.30 and 4.97 ± 0.82 at 1 kHz and 1 MHz, respectively). Some of this increase is attributed to the reduced crosslinking discussed above. However, most of the enhancement observed for the dielectric constant is attributed to the presence of the Janus particles and their gold caps.

Chapter 7 presents the first actuation experiments performed on a dielectric elastomer with surface-anisotropic spherical fillers using a 3D surface profiler. JP SiO_2-loaded p(EGPEA) films show a high compressive response at low electric fields (85% at 12 V/m) resulting in an increased electrostictive coefficient ($S_{exp,JP\ SiO2\text{-}p(EGPEA)}$ = 54.59 × 10^{-16} m^2/V^2), due to their lower Young's Modulus and higher dielectric constant compared to the pure and the SiO_2-loaded p(EGPEA) films ($S_{exp,p(EGPEA)}$ = 0.69 × 10^{-16} m^2/V^2 and $S_{exp,SiO2\text{-}p(EGPEA)}$ = 2.36 × 10^{-16} m^2/V^2). Using the ε_r and Young's Modulus values obtained in Chapters 5 and 6, a theoretical electrostrictive coefficient of $S_{theo,\ JP\ SiO2\text{-}p(EGPEA)}$ = 0.25 × 10^{-16} m^2/V^2 is predicted compared to

S_{theo} = 0.16 × 10^{-16} m^2/V^2 calculated for pure and SiO_2-loaded p(EGPEA) films, respectively. The order of magnitude deviation between S_{theo} value and the S_{exp} value indicates the potential occurrence of other actuation mechanisms such as, for example, electret actuation.

In conclusion, the work reported in this thesis has shown that Janus Particles are good filler materials for dielectric elastomers as they increase the films dielectric constant and lower their Young's modulus. Additional research is needed to characterize the structure of the polymer region surrounding the Janus particles to better understand the fillers' effect on the film structure and the resulting physical properties. In the following, some of these experiments are introduced and discussed briefly.

8-2 Future Works

The work presented in this thesis shows that Janus particles affect the Young's Modulus by softening the polymer matrix and increasing the dielectric constant of the polymer composite. The UV/vis and TGA experiments on pure p(EGPEA) films cured in the presence of glass slides with Ti/Au coating indicate the presence of unpolymerized EGPEA monomer in the films. However, the coating used in these experiments is more than 170 times larger than the amount of Ti/Au-coating in a 0.5 vol% JP SiO_2-loaded p(EGPEA) film. In addition, the experiments performed have not revealed specific information about the molecular structure around the Janus particle fillers. To understand better if the EGPEA monomer and crosslinker react with the gold cap, further experiments with ATR-FTIR are needed giving access to the molecular structure and orientation of molecules at solid interfaces.

Another future experiment should involve the use of pure gold particles and/or SiO_2 particles with two gold caps that coat the entire particle. Comparison of the films containing these symmetric fillers with the anisotropic filler studied here will shine light on the importance of the surface-anisotropic nature of the Janus particles on both the Young's Modulus and the dielectric constant. It will also show whether the surface-anisotropic nature of the Janus particles provides an advantage with respect to aggregation. In addition, these experiments will help to modify the three-component Kerner model[2] such that it can be applied to model and interpret the experimental result of the overall dielectric constant of JP SiO_2-loaded p(EGPEA) films.

As discussed in Chapter 7, the JP SiO_2-loaded p(EGPEA) films clearly outperform the pure and SiO_2-loaded p(EGPEA) films, however, their electro-mechanical film-to-film response is not uniform. The observed distribution of actuation behaviors for the JP SiO_2-loaded films maybe a result of a non-uniform Janus particle orientation and dispersion. The Janus particle orientation can be enhanced by application of an external E-field during polymerization of the p(EGPEA) films because the Janus particles alignment in such a field. In addition, preparation of SiO_2 particles with hydrophobic rather than hydrophilic surface properties as used in this thesis will support a more uniform filler distribution.

An interesting side aspect of the UV/vis studies is that the pure p(EGPEA) films can be patterned by the use of gold masks (stronger curing in the areas without gold and less curing in the areas with gold) potentially providing a simpler more direct route to employ pure p(EGPEA) films in practical applications. A patterned film that could act as a dynamic tactile display could be fabricated by using a gold-coated layer as mask during the photo-polymerization of p(EGPEA).

References

Chapter One

(1) Shankar, R.; Ghosh, T. K.; Spontak, R. J. *Soft Matter* **2007**, *3*, 1116.
(2) Zhang, Y. B.-C. a. Q. *MRS Bulletin* **2008**, *33*, 173
(3) Bar-Cohen, Y. *Electroactive Polymer (EAP) Actuators as Artificial Muscles: reality, potential, and challenges*; SPIE Publications: Bellingham.
(4) Einstein, A.; Annalen der Physik **1906**.
(5) Roy D. Kornbluh, R. P., Harsha Prahlad, Annjoe Wong-Foy, Brian McCoy, Susan Kim, Joseph Eckerle and Tom Low *MRS Bulletin* **2012**, *37*, 246.
(6) International Space Missions: **2009**.

Chapter Two

(1) Zhang, Z. C. Q. *MRS Bulletin* **2008**, *33*, 183.
(2) Caravaca, M. A.; Miño, J. C.; Pérez, V. J.; Casali, R. A.; Ponce, C. A. *Journal of Physics: Condensed Matter* **2009**, *21*, 015501.
(3) Pelrine, R.; Kornbluh, R.; Pei, Q.; Joseph, J. *Science* **2000**, *287*, 836.
(4) Ren, W.; Yang, G.; Mukherjee, B. K.; Szabo, J. P. 2004; Vol. 5385, p 395.
(5) Massachusetts Institute of Technology; Material Property Database.
(6) Moreira, D. C.; Sphaier, L. A.; Reis, J. M. L.; Nunes, L. C. S. *Composites Part A: Applied Science and Manufacturing* **2012**, *43*, 304.
(7) Yang, P.; Lieber, C. M. *Science* **1996**, *273*, 1836.
(8) Shankar, R.; Ghosh, T. K.; Spontak, R. J. *Soft Matter* **2007**, *3*, 1116.
(9) Kofod, G.; Sommer-Larsen, P.; Kornbluh, R.; Pelrine, R. *Journal of Intelligent Material Systems and Structures* **2003**, *14*, 787.
(10) Link, S.; Mohamed, M. B.; El-Sayed, M. A. *The Journal of Physical Chemistry B* **1999**, *103*, 3073.
(11) Einstein, A.; Annalen der Physik 1906.
(12) Guth, E. *Rubber Chemistry and Technology* **1938**, *11*, 676.
(13) Guth, E. *Journal of Applied Physics* **1945**, *16*, 20.
(14) Mooney, M. *Journal of Colloid Science* **1951**, *6*, 162.
(15) Affdl, J. C. H.; Kardos, J. L. *Polymer Engineering & Science* **1976**, *16*, 344.
(16) Niitsoo, O.; Couzis, A. *Journal of colloid and interface science* **2011**, *354*, 887.
(17) Bar-Cohen, Y. *Electroactive Polymer (EAP) Actuators as Artificial Muscles: reality, potential, and challenges*; SPIE Publications: Bellingham.
(18) Madden, J. D. W.; Vandesteeg, N. A.; Anquetil, P. A.; Madden, P. G. A.; Takshi, A.; Pytel, R. Z.; Lafontaine, S. R.; Wieringa, P. A.; Hunter, I. W. *Oceanic Engineering, IEEE Journal of* **2004**, *29*, 706.
(19) Zhang, Q. M.; Hengfeng, L.; Martin, P.; Feng, X.; Cheng, Z. Y.; Haisheng, X.; Cheng, H. *Nature* **2002**, *419*, 284.
(20) Huang, C.; Zhang, Q. M.; Su, J. *Applied Physics Letters* **2003**, *82*, 3502.
(21) Gilbert, L. J.; Schuman, T. P.; Dogan, F. *Ceram. Trans.* **2006**, 179, 17–26

(22) Dang, Z. M.; Zhou, T.; Yao, S. H.; Yuan, J. K.; Zha, J. W.; Song, H. T.; Li, J. Y.; Chen, Q.; Yang, W. T.; Bai, *J. Adv. Mater.* **2009**, 21, 2077–2082
(23) Jiang, S.; Chen, Q.; Tripathy, M.; Luijten, E.; Schweizer, K. S.; Granick, S. *Advanced Materials* **2010**, *22*, 1060.
(24) Casagrande, C.; Fabre, P.; Raphaël, E.; Veyssié, M. *EPL (Europhysics Letters)* **1989**, *9*, 251.
(25) Foss, C. A.; Hornyak, G. L.; Stockert, J. A.; Martin, C. R. *J. Phys. Chem.* **1992**, *96*, 7497.
(26) Takei, H.; Shimizu, N. *Langmuir* **1997**, 13, 1865.
(27) Crowley, J. M.; Sheridon, N. K.; Romano, L. *J. Electrostat.* **2002**, 55, 247
(28) Gangwal, S.; Cayre, O. J.; Bazant, M. Z.; Velev, O. D. *Phys. Rev. Lett.* **2008**, 100, 058302
(29) Pawar A. B.; I. Kretzschmar, I. *Macromolec. Rapid Comm*., **2010**, 31, 150-168.

Chapter Three

(1) Madden, J. D. W.; Vandesteeg, N. A.; Anquetil, P. A.; Madden, P. G. A.; Takshi, A.; Pytel, R. Z.; Lafontaine, S. R.; Wieringa, P. A.; Hunter, I. W. *Oceanic Engineering, IEEE Journal of* **2004**, *29*, 706.
(2) Gangwal, S.; Cayre, O. J.; Velev, O. D. *Langmuir* **2008**, *24*, 13312.
(3) L. Hong, A. C., E. Luijten, and S. Granick *Langmuir* **2008**, *24*, 621.
(4) Kuncova-Kallio, J.; Kallio, P. J. *Conference proceedings : ... Annual International Conference of the IEEE Engineering in Medicine and Biology Society. IEEE Engineering in Medicine and Biology Society. Conference* **2006**, *1*, 2486.
(5) Buguin, A.; Li, M.-H.; Silberzan, P.; Ladoux, B.; Keller, P. *Journal of the American Chemical Society* **2006**, *128*, 1088.

Chapter Four

(1) Produe Univeisity Website http://www.purdue.edu/rem/rs/sem.htm.
(2) Gabbott, P **2008** *Principles and Applications of Thermal Analysis* Wiley
(3) Optoelectronics Technology Co., Ltd. http://www.eray-tech.com/img/alq3_tga.gif
(4) Zhong, Q.; Inniss, D. *Surface Science Letters* **1993,** 290, 1–2, 688–692
(5) Menard, K. P. **1999** *Dynamic Mechanical Analysis: A Practical Introduction* CRC PressINC
(6) Oliver, W. C.; Pharr, G. M. *Journal of Materials Research* **2004**, *19*, 3.
(7) http://www.nanoindentation.cornell.edu/Machine/commercial_machine.htm; The nanoindentation.
(8) Oliver, W. C.; Pharr, G. M. *Journal of Materials Research* **1992**, *7*, 1564.
(9) Jaffe, B; *Piezoelectric Ceramics* Academic Press London and New Yok
(10) Nalwa, H. S., **1999** *Handbook of Low and High Dielectric Constant Materials and Their Applications*, 2, 1-2
(11) Carver, G. P.; **1981** *A manual wafer probe station for an integrated circuit test system*, University of Michigan Library
(12) Sayers, M.W., Gillespie, T.D., and Queiroz, C.A.V. **1986**, *The International Road Roughness Experiment*, World Bank Technical Paper Number 45, The World Bank, Washington, DC.

Chapter Five

(1) Fu, S.-Y.; Feng, X.-Q.; Lauke, B.; Mai, Y.-W. *Composites Part B: Engineering* **2008**, *39*, 933.
(2) Stoyanov, H.; Carthy, D. M.; Kollosche, M.; Kofod, G. *Applied Physics Letters* **2009**, *94*, 232905.
(3) Guth, E. *Journal of Applied Physics* **1945**, *16*, 20.
(4) Bae, J.; Glogowski, E.; Gupta, S.; Chen, W.; Emrick, T.; Russell, T. P. *Macromolecules* **2008**, *41*, 2722.
(5) Muriel, M.; Dubault, A.; Halary, J. L. *Polymer International* **2007**, *56*, 214.
(6) Coquelle, E.; Bossis, G.; Szabo, D.; Giulieri, F. *J Mater Sci* **2006**, *41*, 5941.
(7) Risse, S.; Kussmaul, B.; Krüger, H.; Kofod, G. *Advanced Functional Materials* **2012**, *22*, 3958.
(8) Au, C.; Büyüköztürk, O. *Engineering Fracture Mechanics*, **2006** 73, 3, 348–365
(9) Xia, Y.; Gates, B.; Yin, Y.; Lu, Y. *Advanced Materials* **2000**, *12*, 693.
(10) Mietta, J. L.; Ruiz, M. M.; Antonel, P. S.; Perez, O. E.; Butera, A.; Jorge, G.; Negri, R. M. *Langmuir* **2012**, *28*, 6985.
(11) Nurazreena; Hussain, L. B.; Ismail, H.; Mariatti, M. *Journal of Thermoplastic Composite Materials* **2006**, *19*, 413.
(12) Zaïri, F.; Naït-Abdelaziz, M.; Woznica, K.; Gloaguen, J.-M. *European Journal of Mechanics - A/Solids* **2005**, *24*, 169.
(13) "Elastic Properties and Young Modulus for some Materials". The Engineering ToolBox. Retrieved 2012-01-06.
(14) Premnath, V.; Bellare, A.; Merrill, E. W.; Jasty, M.; Harris, W. H. *Polymer* **1999**, *40*, 2215.
(15) Kumar, V.; Krishnan, S.; Steiner, C.; Maldarelli, C.; Couzis, A. *The Journal of Physical Chemistry B* **1998**, *102*, 3152.
(16) Griffiths, P. R. **2006.** *Beer's Law. Handbook of Vibrational Spectroscopy*.

Chapter Six

(1) Bae, J.; Glogowski, E.; Gupta, S.; Chen, W.; Emrick, T.; Russell, T. P. *Macromolecules* **2008**, *41*, 2722.
(2) Johnson, P. B.; Christy, R. W. *Physical Review B* **1972**, *6*, 4370.
(3) L. Novotny and B. Hecht, *Principles of Nano-Optics*; Cambridge **2006**.
(4) Link, S.; Mohamed, M. B.; El-Sayed, M. A. *The Journal of Physical Chemistry B* **1999**, *103*, 3073.
(5) Levy, O.; Stroud, D. *Physical Review B* **1997**, *56*, 8035.
(6) DuPond website. http://www2.dupont.com/Kapton/en_US/assets/downloads/pdf/summaryofprop.pdf
(7) Simon M. Sze, K. K. N. *Physics of Semiconductor Devices, 3rd edn*; Wiley: New Jersey, 2007.
(8) Morales-Acosta, M. D.; Quevedo-López, M. A.; Gnade, B.; Ramírez-Bon, R. *J Sol-Gel Sci Technol* **2011**, *58*, 218.

Chapter Seven

(1) Shankar, R.; Ghosh, T. K.; Spontak, R. J. *Soft Matter* **2007**, *3*, 1116.
(2) Bar-Cohen, Y. *Electroactive Polymer (EAP) Actuators as Artificial Muscles: reality, potential, and challenges*; SPIE Publications: Bellingham.
(3) Zhang, Q. M.; Hengfeng, L.; Martin, P.; Feng, X.; Cheng, Z. Y.; Haisheng, X.; Cheng, H. *Nature* **2002**, *419*, 284.
(4) Zhang, Z. C. Q. *MRS Bulletin* **2008**, *33*, 183.
(5) Brochu, P.; Pei, Q. *Macromolecular Rapid Communications* **2010**, *31*, 10.
(6) Diaconu, I.; Dorohoi, D. O.; Topoliceanu, F. *Sensors Journal, IEEE* **2006**, *6*, 876.
(7) A. Maliakal J.Q. Cui, I. K., L. Zhu *PMSE Preprints* **2008**, *98*, 169.
(8) Bauer, S.; Gerhard-Multhaupt, R.; Sessler, G. M. *Physics Today* **2004**, *57*, 37.

Chapter Eight

(1) Guth, E. *Journal of Applied Physics* **1945**, *16*, 20.
(2) Kerner, E. H. *Proceedings of the Physical Society. Section B* **1956**, *69*, 808.